NASA TECHNICAL NOTE

NASA TN D-5078

c. 1

NASA TN D-5078

POSSIBLE APPLICATIONS OF THE CONTINUITY-EQUATION PLASMA OSCILLATION TO PULSARS AND OTHER PERIODIC ASTROPHYSICAL PHENOMENA

by J. Reece Roth

Lewis Research Center
Cleveland, Ohio

NATIONAL AERONAUTICS AND SPACE ADMINISTRATION • WASHINGTON, D. C. • MARCH 1969

POSSIBLE APPLICATIONS OF THE CONTINUITY-EQUATION PLASMA OSCILLATION TO PULSARS AND OTHER PERIODIC ASTROPHYSICAL PHENOMENA

By J. Reece Roth

Lewis Research Center
Cleveland, Ohio

NATIONAL AERONAUTICS AND SPACE ADMINISTRATION

For sale by the Clearinghouse for Federal Scientific and Technical Information
Springfield, Virginia 22151 – CFSTI price $3.00

ABSTRACT

The continuity equations for neutral and charged particles in a partly ionized gas may possess periodic solutions. These oscillations are suggested as a possible clock mechanism for periodic astrophysical phenomena such as geomagnetic micropulsations, pulsars, and of long-period fluctuations in the charged particle density of the interstellar medium. A mathematical model of these oscillations is derived and applied to two cases of astrophysical interest; an isolated, virtually uniform region of partially ionized gas; and a slightly ionized stellar or planetary atmosphere, the characteristics of which vary with position. The theoretical analysis is supplemented by an experimental investigation of the pulsed production and loss of electrons from a magnetically confined laboratory plasma which was subject to the continuity-equation oscillation. Some pulsar-like characteristics were observed and measured in this plasma.

CONTENTS

POSSIBLE APPLICATIONS OF THE CONTINUITY-EQUATION PLASMA OSCILLATION TO PULSARS AND OTHER PERIODIC ASTROPHYSICAL PHENOMENA

by J. Reece Roth

Lewis Research Center

SUMMARY

The continuity equations for neutral and charged particles in a partly ionized gas may possess periodic solutions. These oscillations are suggested as a possible clock mechanism for periodic astrophysical phenomena such as geomagnetic micropulsations, pulsars, and long-period fluctuations in the charged particle density of the interstellar medium. Analytical and experimental investigations of this oscillation are discussed in light of their possible astrophysical relevance. A mathematical model is derived which exhibits such oscillations. The physical conditions that must occur in order that this model be a reasonable approximation are examined.

The most restrictive of these conditions is that a population of energetic electrons, about 100 electron volts in energy, must permeate the partially ionized gas in question; that the ionization mean free paths be larger than the minimum characteristic dimensions of the oscillating region, and that the product of time-averaged electron and neutral number densities, $\hat{n}_e\hat{n}$, be independent of position within the coherently oscillating region.

The particular model of these oscillations which is discussed is applied to two cases of astrophysical interest. The first is an isolated, spatially uniform region of partially ionized gas, the characteristics of which are intended to be representative of interstellar H-I and H-II regions. The second case is one in which the electron and neutral number density may vary significantly with position, as would be the case in a planetary atmosphere or the upper reaches of a stellar atmosphere. It is shown that the physical conditions existing in these two cases may satisfy the conditions necessary to make the oscillation possible.

Exact solutions to the nonlinear continuity equations were obtained on an analog computer. It was found that the electron number density waveform displayed the pulsar-like characteristic of sharp, narrow, periodic peaks between broad, flat minima. If a turbulent heating process or fluctuating electric fields were available to heat these pulses of electrons to relativistic energies, the pulses of electrons may well be accompanied by pulsed radio-frequency radiation.

An experimental program was undertaken to study the pulsed emission of electrons observed from a laboratory plasma subject to the continuity-equation oscillation. Some suggestive characteristics have been observed and measured in this laboratory plasma, including the following: (1) long-term stability of the pulse frequency within limits set by apparatus limitations; (2) observation of fine structure in the pulses of electron emission; and (3) the frequency of the bursts was observed to vary over the range $87 \leq \nu \leq 10^5$ hertz. Much lower frequencies are to be expected in an astrophysical context, as a consequence of the lower particle densities characteristic of such applications.

INTRODUCTION

Periodic pulses of radio-frequency (RF) emission have recently been observed emanating from sources in interstellar space (refs. 1 to 3). These pulses have been observed to have the following characteristics:

(1) The pulses of RF emission have an extremely stable period, constant to one part in 10^6 or 10^7 (refs. 1 and 2).

(2) Several periodic sources have been observed, the pulse frequencies of which are about 1.0 hertz.

(3) This periodic RF emission has been received over frequencies from about 40 to 600 megahertz (ref. 2).

(4) The flux intensity appears to fall off with frequency according to a $\nu^{-1.5}$ power law (ref. 2).

(5) The RF radiation from these sources has been observed to be highly polarized (ref. 3).

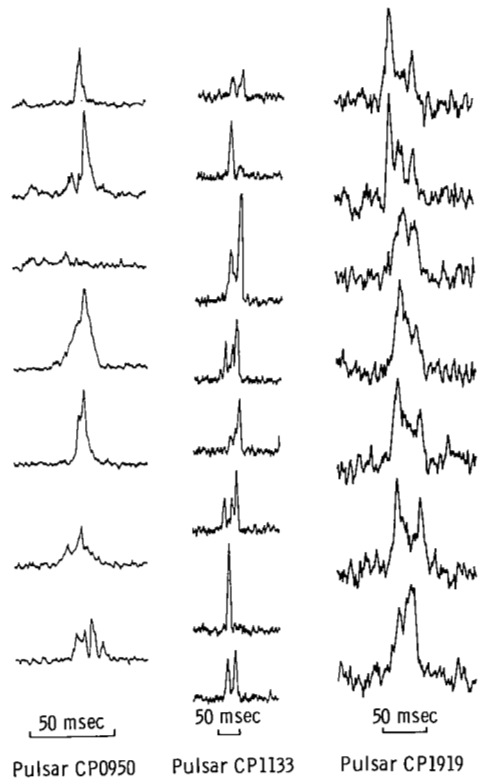

Figure 1. - Typical consecutive pulse waveforms for three pulsars, taken from reference 6. Waveforms were observed at frequency of 408 megahertz with bandwidth of 4 megahertz and time constant of 1 millisecond.

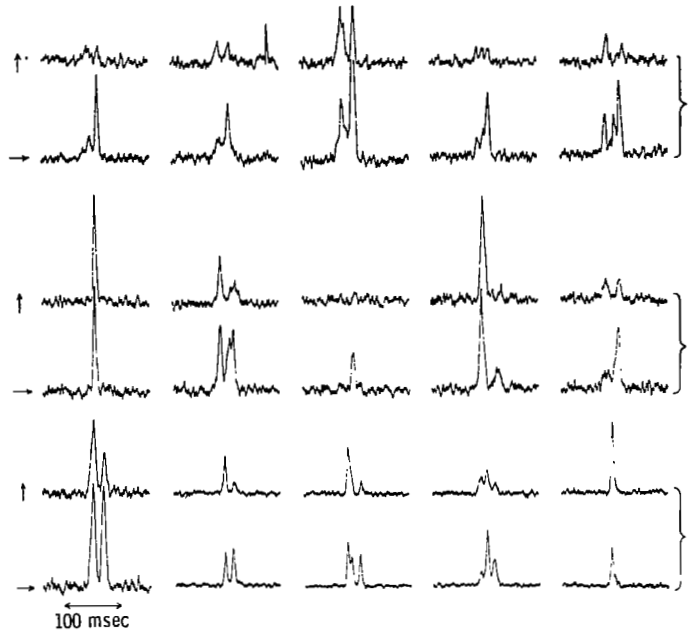

Figure 2. - Output of two receivers at 408 megahertz which were connected to orthogonal dipoles, as reported in reference 3. Pulsar CP1133 was under observation. Note instances of strong polarization of received signal.

(6) Periodic optical emission has not been observed from a pulsar, the presumed optical image of which has been studied (ref. 4).

(7) The individual pulses of RF emission have a fine structure (refs. 5 to 7).

(8) The leading edge of the RF pulse appears to have a rise time of 1 millisecond or less (refs. 5, 6, and 8).

On figure 1 is shown a series of consecutive pulses, at a frequency of 408 megahertz, for three sources (taken from ref. 6, p. 327). On figure 2 is shown pulses at 408 megahertz from the source CP 1133, taken for two perpendicular components of radio frequency polarization (fig. 2 of ref. 3).

When taken together, the above characteristics are quite puzzling, and cannot be readily explained in terms of a physical model the existence of which is known on the basis of independent observational evidence (refs. 2 and 9). It appeared to the author that the continuity-equation oscillation mechanism might be capable of providing a periodic, clock-like mechanism for the production of electrons. The observed RF pulses may result from the stochastic heating and synchrotron radiation of such pulses of electrons.

Several entirely distinct physical models are capable of yielding a coupled pair of continuity equations that possess periodic solutions (ref. 10). A general model for astrophysical applications is shown in figure 3. It is assumed that the oscillating region is

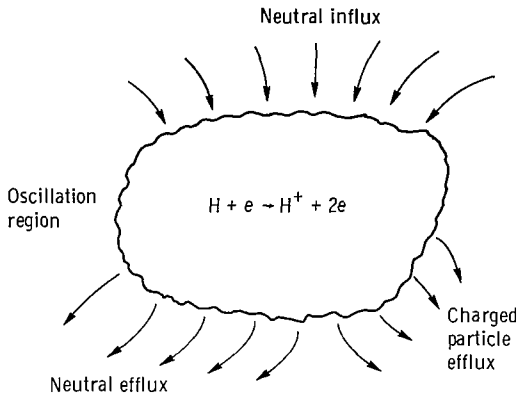

Figure 3. - Schematic of region of partially ionized gas subject to continuity-equation oscillation. Such a region ionizes a small fraction of the neutrals streaming through it. Time delays associated with motion of neutrals across region give rise to time-dependent net efflux of charged particles from region, as discussed in appendixes B and C.

populated by electrons sufficiently energetic to ionize the neutral gas within it. The ambient neutral gas can be conceptually divided into two categories: (1) Neutral gas that passes through the oscillating region without being ionized, shown on the top of figure 3, and (2) a small fraction of this neutral flux that interacts in the oscillating region during each cycle of oscillation. The electrons and ions produced in the oscillating region are either lost to space or recombine in the surroundings. Photoionization and three-body recombination processes are assumed either to be not present in this model, or, if present, to be in balance.

In the model of figure 3 it is important to note that at any instant of time there is not a detailed balance between the oscillating flux of charged particles leaving the region of interest, and the virtually constant flux of neutrals entering it. The time delay associated with the transit of neutral particles across the oscillating region acts as an averaging mechanism that prevents a detailed balance at any point within the ionized gas, and makes possible a relaxation oscillation of the charged particle number density within it. This physical process will be elucidated in the subsequent discussion.

The present author has analyzed a physical model similar to that of figure 3, which yields continuity equations identical to those to be derived below (refs. 10 and 11). The synchronous charged particle number density oscillations predicted by these analyses were observed in the author's laboratory under conditions that roughly simulate the astrophysical case (refs. 12 and 13). The simultude with the astrophysical case became even more suggestive when it was observed that the discharge in question was emitting pulses of charged particles with the continuity-equation frequency.

THEORETICAL ANALYSIS

Relevant Results of Prior Investigations

Periodic solutions were obtained in reference 10 to the following pair of coupled, nonlinear differential equations

$$\dot{n} = C_0 + C_1 n + C_2 n_e + C_3 n n_e + C_4 n^2 + C_5 n_e^2 \tag{1}$$

$$\dot{n}_e = A_0 + A_1 n + A_2 n_e + A_3 n n_e + C_4 n^2 + C_5 n_e^2 \tag{2}$$

in the small amplitude limit, $n(t) = \hat{n} + \delta n(t)$, where $\delta n(t) \ll \hat{n}$. The peak-to-peak amplitude of $n_e(t)$ may be large or small compared with the average value of $n_e(t)$. The coefficients A_i and C_i of these equations are capable of representing the most commonly encountered sources and sinks which appear in the neutral and charged particle continuity equations, with the exception of diffusion and three-body processes.

These equations are written on the assumption that the Debye distance is smaller than the plasma dimensions, thus enabling one to eliminate either the ion or the electron continuity equation as an independent constraint on the oscillation. They also assume that the diffusion term is negligible, or may be represented by one of the coefficients A_i or C_i. This assumption is justified in appendixes B and C.

In reference 10 it was shown that the small-amplitude solution for $n_e(t)$ of the two equations (1) and (2) has a waveform given by Jacobian elliptic functions. These solutions are plotted on figures 4(a) to (c) for three particular cases. Figure 4(a) displays the sharp, isolated peaks separated by broad, flat minima that is characteristic of the Jacobian elliptic functions for large peak-to-peak amplitudes.

In references 12 and 13 it was shown that the discharge under experimental investigation in these references could be adequately described by specializing equations (1) and (2) to the following form

$$\dot{n} = \hat{n}_e n \langle \sigma v \rangle_{ne} - n_e n \langle \sigma v \rangle_{ne} \tag{3}$$

$$\dot{n}_e = -\hat{n} n_e \langle \sigma v \rangle_{ne} + n n_e \langle \sigma v \rangle_{ne} \tag{4}$$

where $\hat{n}_e$ and $\hat{n}$ are, respectively, the time and space averaged electron and neutral number density in the oscillating region. $\langle \sigma v \rangle_{ne}$ is the ionization rate parameter for

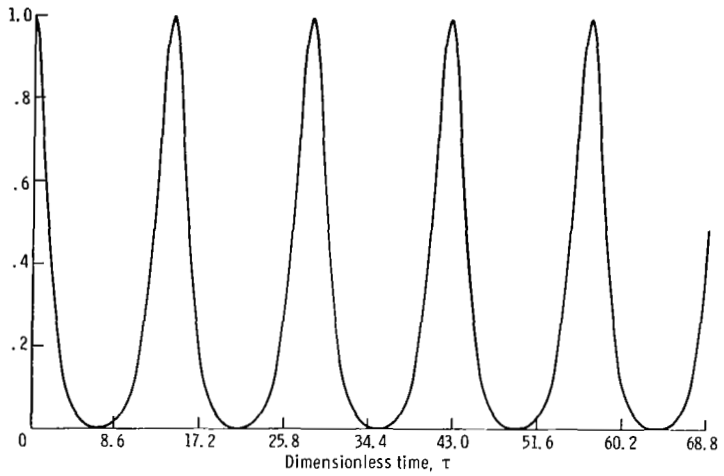

(a) $\eta_s = 0.6667$.

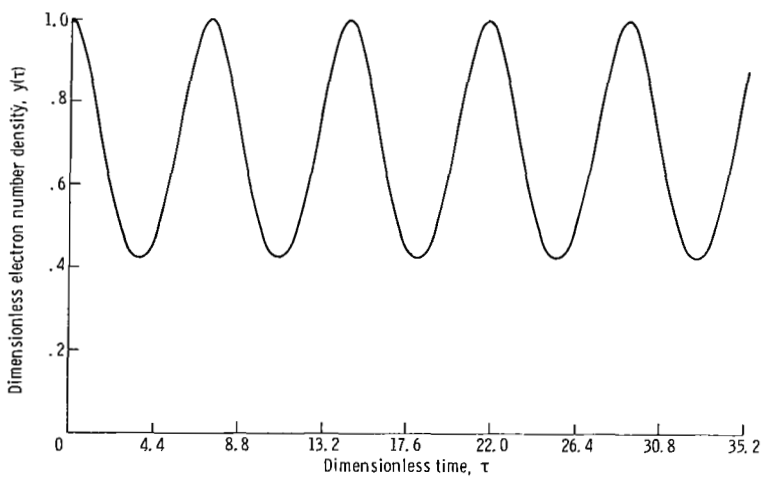

(b) $\eta_s = 0.75$.

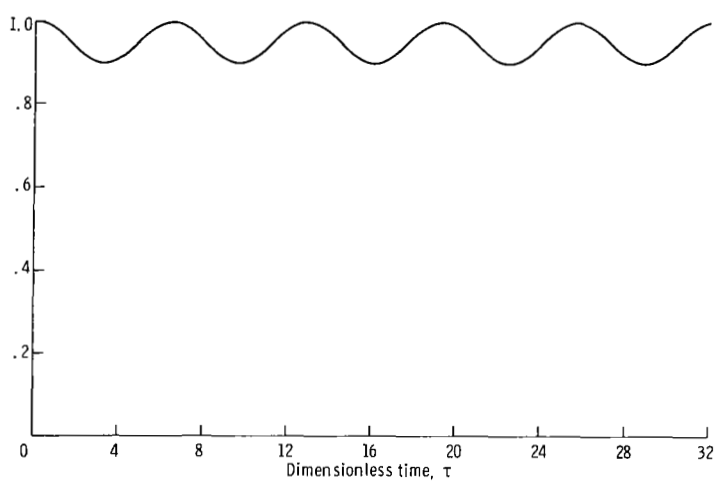

(c) $\eta_s = 0.95$. (Note departure from sinusoidal waveform as peak-to-peak amplitude becomes large.)

Figure 4. - Waveform of dimensionless electron number density as given by small-amplitude approximation for three amplitude indexes η_s.

electron-neutral ionization. In these references it was shown that the electron and neutral number densities are oscillating, with a frequency that is approximately

$$\nu = \frac{\sqrt{\hat{n}_e \hat{n}}\ \langle \sigma v \rangle_{ne}}{2\pi} \text{ Hz} \tag{5}$$

when the peak-to-peak amplitude of $n_e(t)$ is not comparable to its maximum value. The reader is referred to references 11 and 13 for a discussion of the case in which the peak-to-peak amplitude of $n_e(t)$ is comparable to its maximum value. In references 12 and 13, it is shown that the oscillations observed in an appropriate experimental situation obeyed the theory based on small-amplitude solutions to equations (3) and (4).

These equations are not adequate if photoionization and three-body recombination processes are present in the region of interest, or if these processes are not in balance at all times. In some real cases, one might expect to find processes which demand consideration of the momentum or energy equations, or which involve time-dependent electric or magnetic fields. The experimental results presented in reference 13 bear out the assumption that the electric and magnetic fields do not determine the frequency, amplitude, or waveform of the continuity-equation oscillation.

In an astrophysical context, the second terms on the right-hand side of equations (3) and (4) represent, respectively, the instantaneous rate at which neutrals are lost, and charged particles are produced, by electron-neutral impact ionization. It is shown in appendixes B and C that a consideration of the divergence term of the continuity equations will yield the first terms appearing on the right-hand side of equations (3) and (4), provided that the ionization mean free paths of electrons and neutrals are both larger than the minimum dimensions of the oscillating region, such that Fick's law is not valid.

Requirements for Coherent, Periodic Oscillations

In this section, the requirements will be discussed which must be met if this model of the oscillation process is to occur in an astrophysical context. The requirements which must be satisfied merely in order to make an analytical treatment possible will be discussed in the next section.

The basic physical process responsible for the oscillations under discussion is the time-dependent rate of ionization of neutrals by energetic electrons. The ionization-rate coefficient, $\langle \sigma v \rangle_{ne}$, for this process is significant above an electron kinetic temperature of about 10 electron volts, and attains its maximum in the energy range from 80 to 400

electron volts. For neutral atoms of astrophysical interest, the ionization rate coefficient varies by less than a factor of 2 from about 50 electron volts to 1 kiloelectron volts (refs. 14 and 15). In order for this ionization process to take place, there must exist a significant population of energetic electrons whose kinetic temperatures are above the ionization potential of the ambient neutral gas.

An inspection of equation (5) suggests that a necessary condition for coherent oscillations due to this mechanism is that the density product $\hat{n}_e\hat{n}$ be constant in the region of coherent oscillation. The exact outcome of the continuity-equation oscillation for nonuniform $\hat{n}_e\hat{n}$ is not known. Presumably a synchronizing effect exists which can keep the oscillation coherent over minor variations from uniformity, since coherent oscillations were observed in the experiment described below when $\hat{n}_e\hat{n}$ varied by a factor of 10 over the discharge volume. If this product were to vary greatly with position, different regions may oscillate with different frequencies, and the oscillations in $n_e(t)$ would then be observed to be broad-band and incoherent.

It is not difficult to see that the entire region can oscillate coherently if the electrons move across the characteristic dimension L of the oscillation region in a time less than the period of oscillation, T,

$$t_{oe} < T \tag{6}$$

However, this is not a necessary condition, as is discussed below in the section Synchronization of Pulsating Region. If the electrons have energy V_e and velocity v_e, we may use equation (5) to write equation (6) in the following form,

$$\frac{L}{v_e} < \frac{1}{\nu} = \frac{2\pi}{\sqrt{\hat{n}_e\hat{n}}\,\langle\sigma v\rangle_{ne}} \tag{7}$$

For observed pulsar frequencies of about 1.0 hertz, equation (7) suggests that the maximum characteristic dimension L for 100 electron volts electrons must be less than 6000 kilometers if this condition is to be satisfied.

A necessary condition for the existence of synchronous oscillations is that the mean free time of the electrons in the oscillating region must be less than the period, if the peak-to-peak amplitude of the electron density is comparable to its maximum value. The electron mean free time is just

$$t_{ne} = \frac{1}{\hat{n}\langle\sigma v\rangle_{ne}} \tag{8}$$

The requirement that this be less than the continuity equation period T is then expressed by

$$\frac{1}{\hat{n}\langle \sigma v \rangle_{ne}} < \frac{2\pi}{\sqrt{\hat{n}_e \hat{n}}\ \langle \sigma v \rangle_{ne}} \tag{9}$$

This may be rewritten in terms of the inequality

$$\frac{1}{2\pi} \sqrt{\frac{\hat{n}_e}{\hat{n}}} < 1 \tag{10}$$

This requirement is satisfied whenever the gas is partially ionized, such that $\hat{n}_e \ll \hat{n}$.

Requirements for Analytical Treatment

A number of additional assumptions are desirable in order to facilitate an analytical derivation of the oscillations in question. The first such assumption is that the peak-to-peak amplitude of the fluctuations in neutral density is small by comparison with the average neutral density. This assumption also implies that $\hat{n}_e \ll \hat{n}_o$, since there is an electron gained for each neutral lost. A second assumption that will be quite convenient during the course of the analysis below is that the electron or neutral velocity distribution is monoenergetic or unidirectional. This should cause no difficulty in principle, since one can relate the assumed monoenergetic or unidirectional velocity to the most probable velocity of an isotropic, Maxwellian distribution.

An attempt to apply the small amplitude approximation to continuity equations which include a diffusion term results in a nonlinear equation for which solutions are not known. One must at present restrict the analytical development to continuity equations without diffusion terms. This means that electrons and neutrals must not be subject to diffusion due to electron-neutral collisions, or that the mean free paths of electrons and neutrals for electron-neutral ionization must be comparable to or longer than the smallest characteristic dimension of the oscillating region. If v is the velocity of the neutral atoms, the mean free path of a neutral for an ionizing collision is

$$\lambda_n = \frac{v}{\hat{n}_e \langle \sigma v \rangle_{ne}} \tag{11}$$

The requirement that this be greater than the characteristic dimension L may be stated

$$L < \frac{v}{\hat{n}_e \langle \sigma v \rangle_{ne}} \tag{12}$$

The companion requirement that the mean free path of the electrons be large compared to the characteristic dimensions may be written

$$L < \frac{v_e}{\hat{n} \langle \sigma v \rangle_{ne}} \tag{13}$$

where v_e is the electron velocity.

In the analysis in appendix B of a spherically symmetric H-I or H-II region, it is convenient to assume that the electron and neutral number densities are spatially uniform, except for the small oscillating spatial perturbations resulting from the periodic ionization process. The neglect of these spatial perturbations for pulsed sources of charged particles is shown to be justified by the excellent agreement of the theory based on this assumption with the experimental results reported in reference 13.

In the study of planetary and stellar atmospheres in appendix C, it is convenient to assume that the constant product $\hat{n}_e \hat{n}$ arises from a neutral density that decreases exponentially with distance above the surface, and an electron density that increases exponentially with distance above the surface, with the same scale height as the neutral atmosphere.

NATURE OF EXACT, OSCILLATORY SOLUTIONS

Nondimensionalization of Equations

It is shown in appendixes B and C that under the assumptions specified in the previous section, the equations of continuity for a partially ionized gas of astrophysical interest may be approximated by a symmetric pair of equations, given by equations (3) and (4),

$$\dot{n} = n(\hat{n}_e - n_e)\langle \sigma v \rangle_{ne} \tag{3}$$

$$\dot{n}_e = -n_e(\hat{n} - n)\langle \sigma v \rangle_{ne} \tag{4}$$

where n and n_e are both functions of time, and may also be functions of position. $\hat{n}_e$ and $\hat{n}$ are the time and space averaged values of the electron and neutral number density.

This pair of equations has long been known to possess oscillating solutions (refs. 16 to 18).

Exact closed-form solutions to these equations have not been obtained, because of their nonlinear nature. It is of some interest to obtain exact solutions numerically and compare the waveform geometry of $n_e(t)$ with, for example, that of the pulsar bursts shown in figures 1 and 2. If we apply the initial conditions

$$\dot{n}_e(0) = 0 \tag{14}$$

$$n_e(0) = n_{eo} \tag{15}$$

to $n_e(t)$, equation (4) then implies that the initial condition on $n(t)$ is

$$n(0) = \hat{n} \tag{16}$$

It should be noted that n_{eo} is an extremal value of $n_e(t)$, and may be either a maximum or minimum of the charged particle density.

It is convenient for purposes of obtaining exact solutions to equations (3) and (4) to define a nondimensional neutral density,

$$x \equiv \frac{n(t)}{\hat{n}} \tag{17}$$

a nondimensional electron density

$$y \equiv \frac{n_e(t)}{n_{eo}} \tag{18}$$

an extremal fraction of ionization,

$$\delta \equiv \frac{n_{eo}}{\hat{n}} \tag{19}$$

and an "amplitude index"

$$\eta_e \equiv \frac{n_e}{n_{eo}} \tag{20}$$

which is the ratio of the time averaged value of $n_e(t)$ to its extremal value. When n_{eo} is chosen as the maximum value of $n_e(t)$, then $y \leq 1.0$, $\eta_e \leq 1.0$, and δ is the maximum fraction ionized. When n_{eo} is chosen as the minimum electron number density, $y \geq 1.0$, $\eta_e \geq 1.0$, and δ is the minimum fraction ionized. It is also useful to define a nondimensional time,

$$\tau = (n_{eo}\hat{n})^{1/2}\langle \sigma v \rangle_{ne} t \tag{21}$$

which will make the frequencies and periods of order unity.

Substituting equations (17) to (21) into equations (3) and (4), one obtains the continuity equations in dimensionless form,

$$\dot{x} = x(\eta_e - y)\delta^{1/2} \tag{22}$$

$$\dot{y} = -y(1 - x)\delta^{-1/2} \tag{23}$$

where the dots now represent a derivative with respect to the dimensionless time τ. This pair of equations can be solved numerically by a computer, or in closed form by using the small amplitude approximation.

Analog Computer Solutions for $n_e(t)$

Equations (22) and (23) were programmed on an analog computer, and the nature of the waveforms of $y(t)$ studied as a function of the amplitude index η_e, and of the maximum fraction of ionization, δ.

The waveform of $y(t)$ is illustrated in figure 5(a) through (k) for $\delta = 0.01$. It is notable that when η_e is near unity, the peak-to-peak amplitude of $y(t)$ is small, and its waveform is sinusoidal. As η_e approaches zero, however, the peak-to-peak amplitude of $y(t)$ approaches unity, and the waveform takes on a characteristic appearance of sharp, narrow peaks, separated by broad, flat minama. These characteristics of the waveforms of $y(t)$ for $\eta_e \leq 0.25$ are particularly suggestive of the pulsar waveforms illustrated in figure 1. Also apparent on figure 5 is the fact that the frequency is a function of the amplitude index η_e, and hence of the peak-to-peak amplitude of $y(t)$. Such a dependence of frequency on amplitude is consistent with the nonlinear nature of equations (22) and (23).

It was found that the peak-to-peak amplitude of the oscillation was not a function of the fraction ionized, δ. This observation is consistent with the predictions of the small-

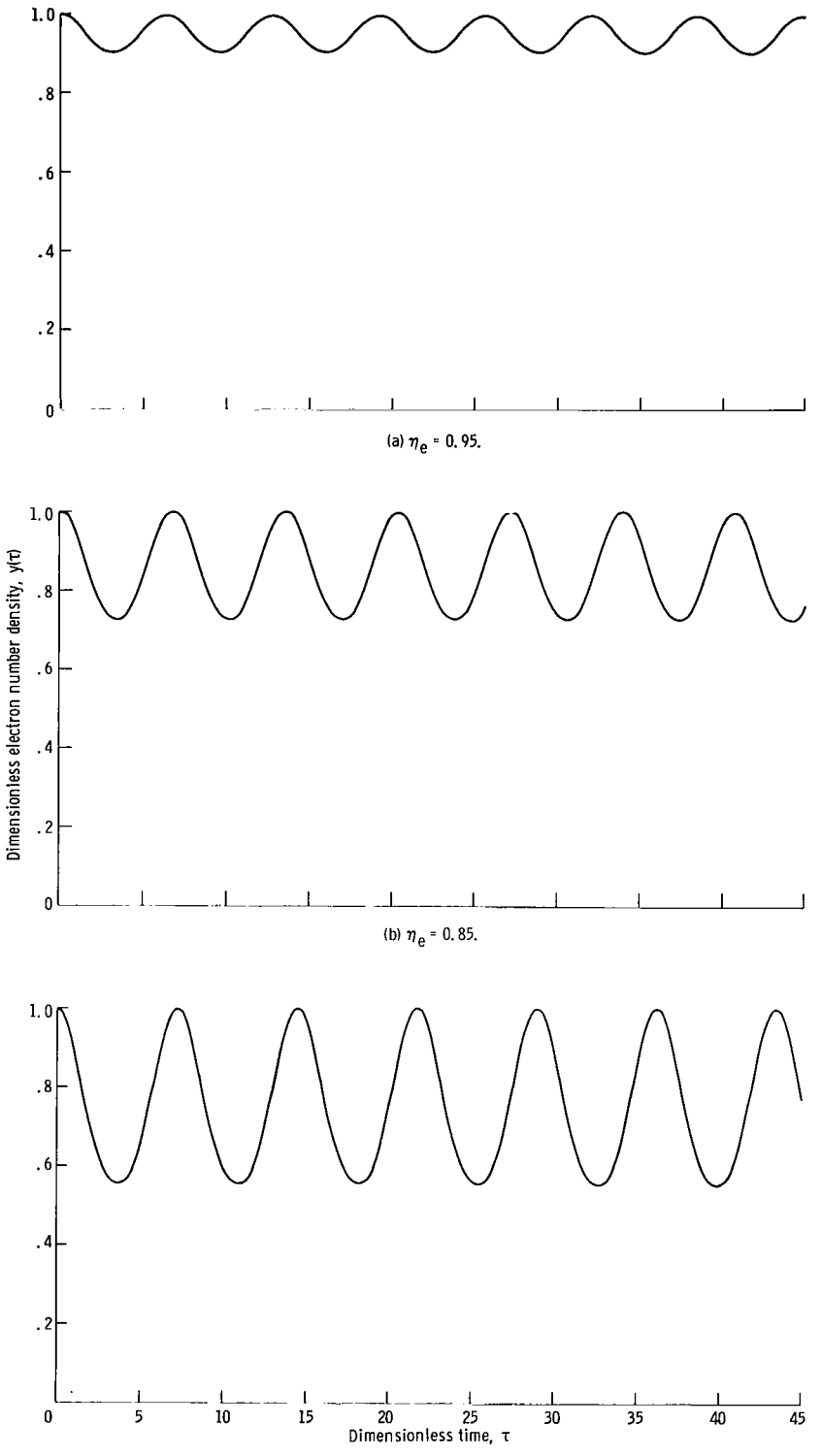

(a) $\eta_e = 0.95$.

(b) $\eta_e = 0.85$.

(c) $\eta_e = 0.75$.

Figure 5. - Waveforms of dimensionless electron number density as function of dimensionless time for selected values of amplitude index η_e. These exact solutions to equations (22) and (23) were obtained on an analog computer for an extremal fraction of ionization of 0.01.

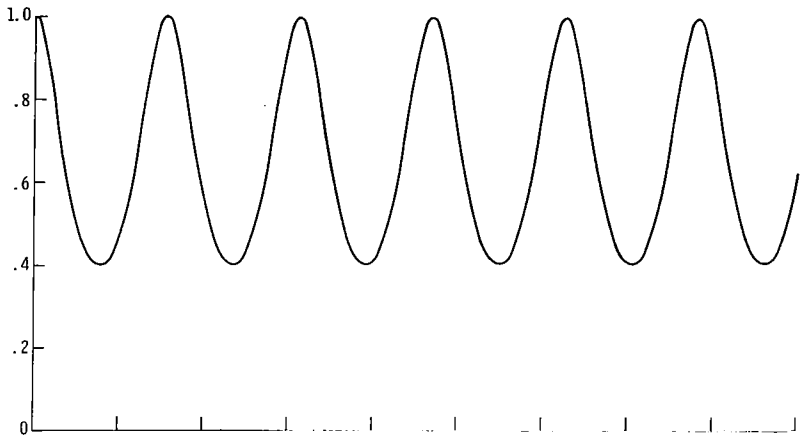

(d) $\eta_e = 0.65$.

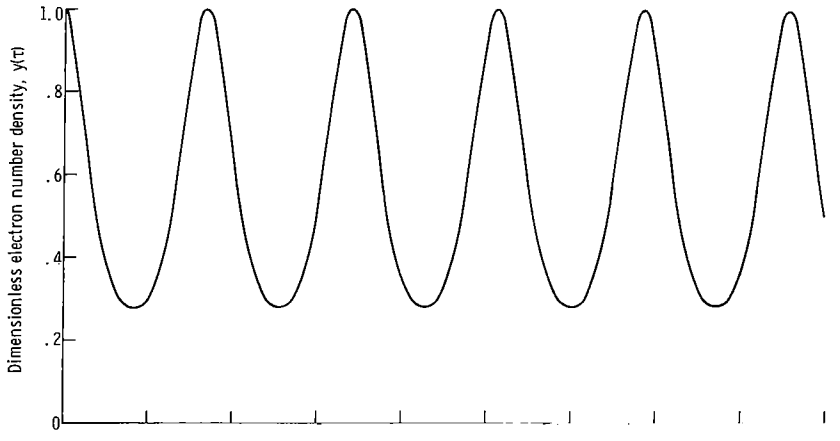

(e) $\eta_e = 0.55$.

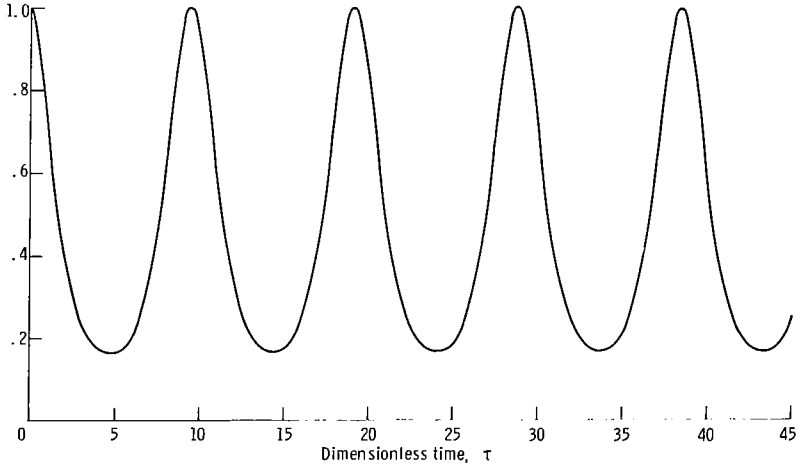

(f) $\eta_e = 0.45$.

Figure 5. - Continued.

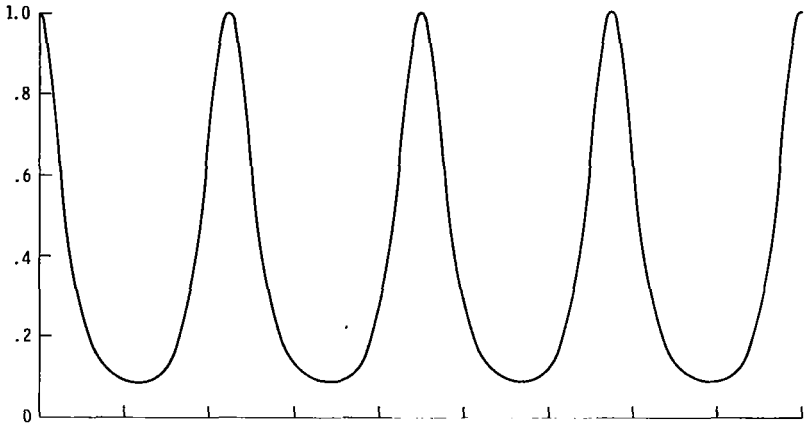

(g) $\eta_e = 0.35$.

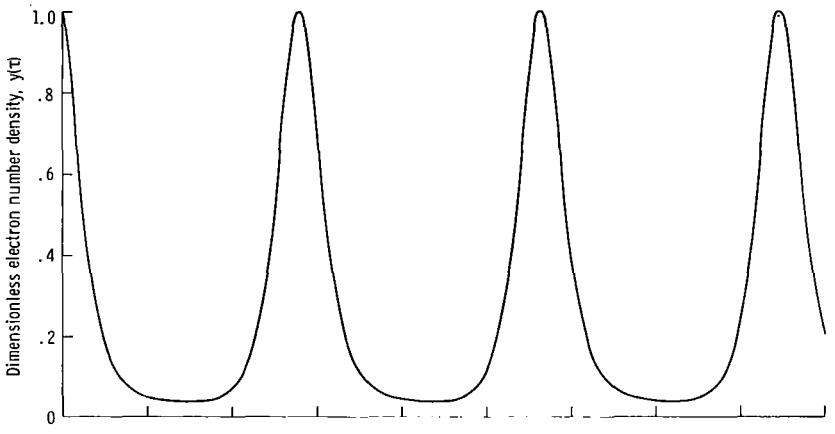

(h) $\eta_e = 0.25$.

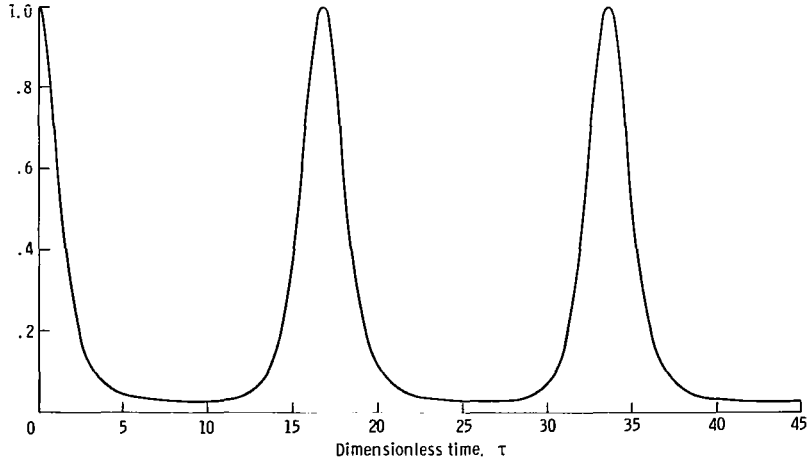

(i) $\eta_e = 0.20$.

Figure 5. - Continued.

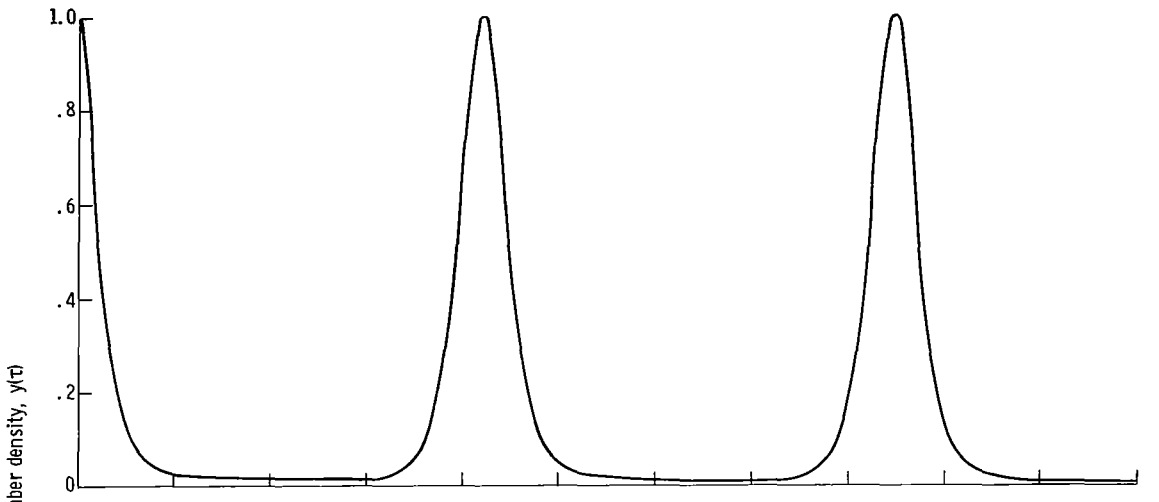

(j) $\eta_e = 0.15$.

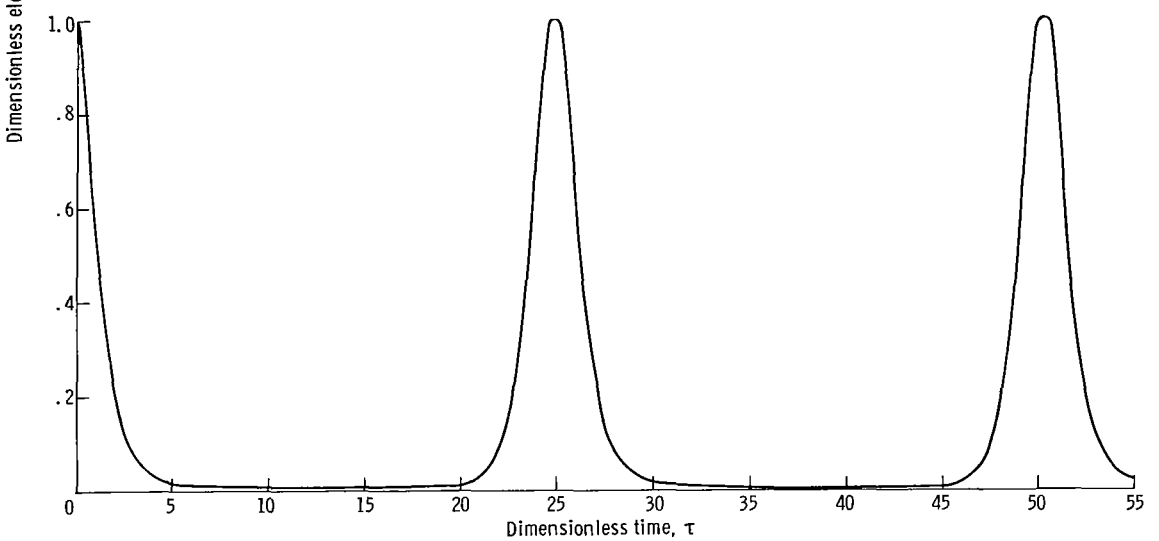

(k) $\eta_e = 0.125$.

Figure 5. - Concluded.

amplitude solution obtained in references 10 and 11. A plot of the peak-to-peak amplitude of y(t), Δy is shown in figure 6 as a function of η_e on the curve labeled "exact."

In figure 7 is shown an exact analog computer solution for the waveform of y(t) as a function of δ when $\eta_e = 0.25$. This figure illustrates the small changes in frequency and geometry of the waveform that result from variation of the fraction ionized, δ, over the range $0.04 \leq \delta \leq 1.0$. The curves for $\delta = 0.04$ and 0.10 are virtually coincident in this figure. It is evident that the peak-to-peak amplitude of y(t) is not a function of δ, and that the frequency increases slightly as δ is varied from 1.0 down to 0.10. There

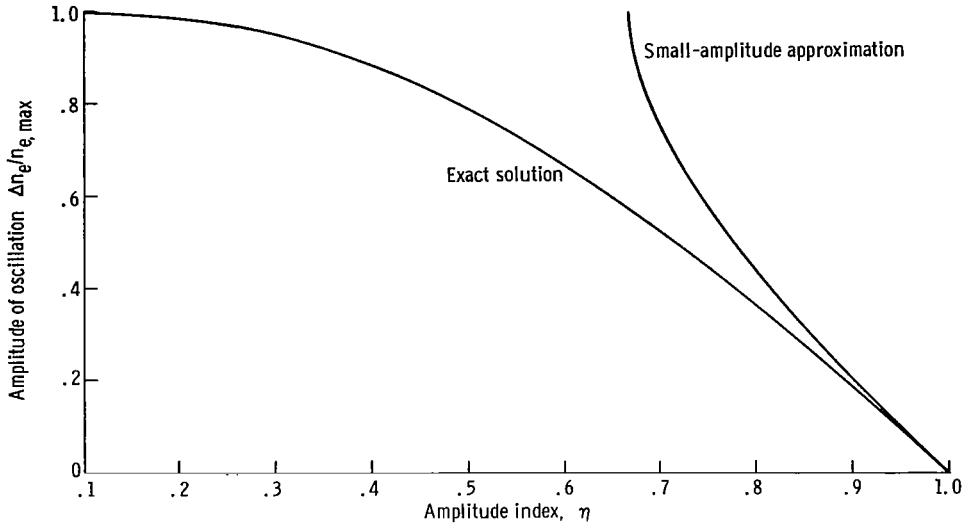

Figure 6. - Peak-to-peak amplitude of oscillation of dimensionless electron number density as function of amplitude index η. The exact results are taken from analog computer data and are not a function of maximum fraction ionized. Small-amplitude results fail below $\eta = 0.80$ because of spurious limit introduced by small-amplitude approximation at $\eta = 2/3$.

are also slight changes in the waveform of y(t) as δ is varied over this range, with the peaks becoming more symmetrical about their maximum as δ is reduced below 1.0. It is clear from figure 7 that there is no significant effect of δ on either the frequency or the geometry of y(t) when δ is below 0.10. One may therefore safely ignore δ as a significant independent variable when the maximum fraction of ionization of a gas is less than 10 percent.

The nondimensionalization of time chosen in equation (21) allows the frequency of oscillation shown in figure 5(a) to (k) to be expressed in the form (ref. 11)

$$\nu = \frac{(\hat{n}_{eo}\hat{n})^{1/2}\langle \sigma v \rangle_{ne}}{2\pi} G(\eta_e, \delta) \tag{24}$$

where $G(\eta_e, \delta)$ accounts for the lowering of the frequency with η_e shown on figure 5. The quantity $G(\eta_e, \delta)$ is shown as a function of η_e in figure 8 for the case $\delta = 1.0$ and $\delta = 0.01$. The latter curve is appropriate for all values of $\delta \leq 0.10$, since $G(\eta_e, \delta)$ is virtually independent of δ for $\delta \leq 0.10$.

A comparison is given in appendix D of these exact analog computer solutions with the small amplitude approximation of references 10 and 11.

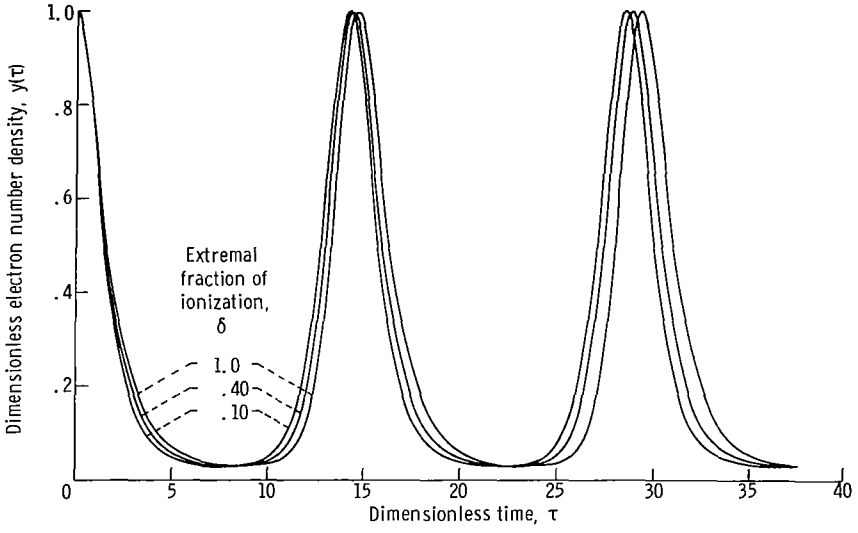

Figure 7. - Exact, analog computer waveforms of dimensionless electron number density for exact amplitude index of 0.25. Small effect of maximum fraction ionized δ on shape of waveform and frequency of oscillation is shown. Note that peak-to-peak amplitude of oscillation is not a function of δ.

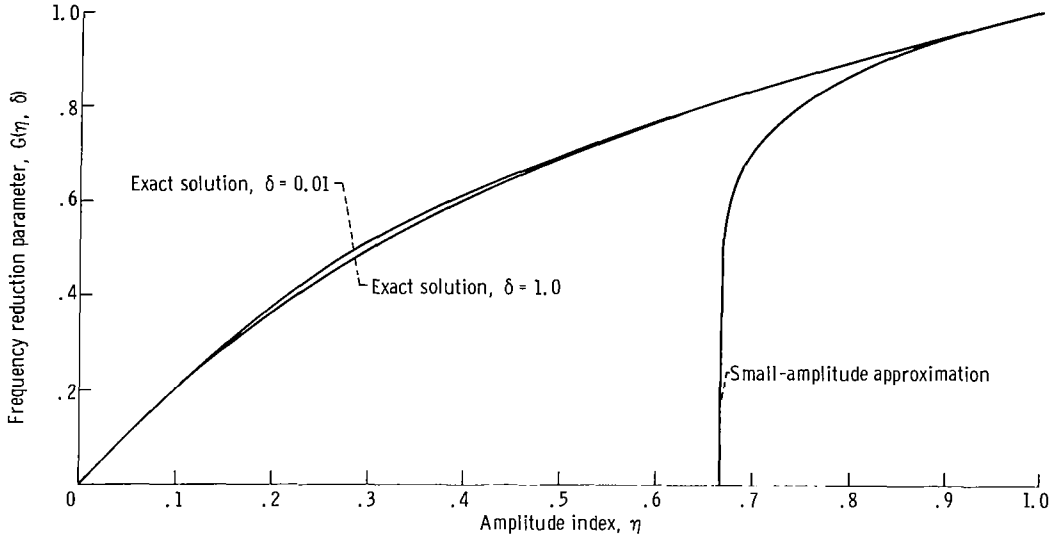

Figure 8. - Frequency reduction parameter $G(\eta, \delta)$ as function of amplitude index η and maximum fraction ionized δ. Exact, analog-computer solutions show small effect of δ on G. Below $\delta = 0.10$, effect is negligible. Value of $G(\eta)$ based on small-amplitude approximation fails below $\eta = 0.80$.

RELEVANT OBSERVATIONS IN A LABORATORY PLASMA

Description of Apparatus and Discharge

The superconducting magnet facility in which the experiments were conducted has been described previously in reference 19. The geometry of the discharge has been described in reference 20, and its properties and operation in references 21 and 22. An isometric cut-away drawing of the discharge and magnetic field coils is shown in figure 9. The plasma is a hot-ion, modified Penning discharge confined in a magnetic mirror geometry with a mirror ratio of 2.5:1. The discharge is located in the center of a 0.85 meter diameter, 1.7 meter long vacuum tank. The magnetic field lines on which the charged particles are confined intersect the tank walls about 50 centimeters outside the discharge. The magnetic mirror existing between the walls and the confining mirrors should act to prevent a backflow of charged particles from the walls to the discharge. The discharge was normally operated with a maximum magnetic field on the axis of 1.0 tesla, and at pressures below 10^{-4} torr. At these pressures, the mean free path of electrons and neutrals for ionization was much larger than the discharge dimensions, a necessary condition for a meaningful simulation of astrophysical phenomena.

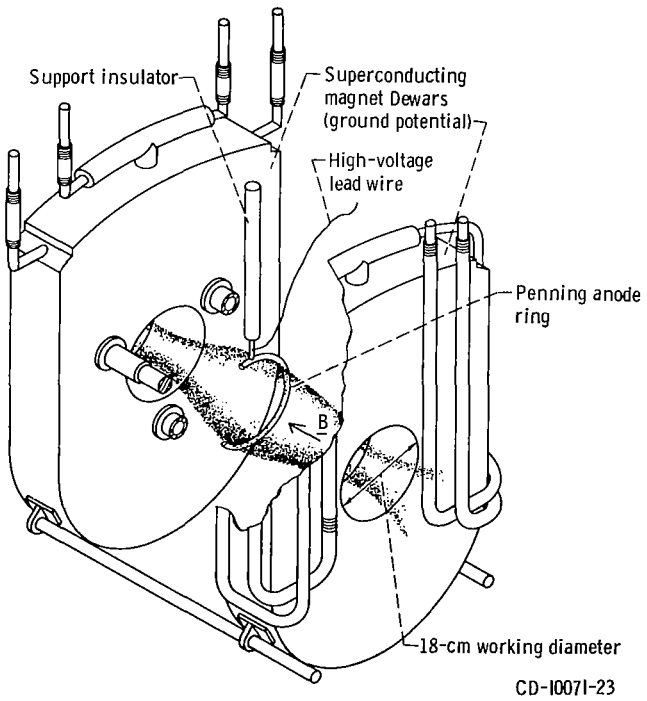

Figure 9. - Isometric, cutaway drawing showing discharge in magnetic mirror, superconducting magnet facility.

Functional Dependence of Frequency on $\hat{n}_e\hat{n}$

The characteristics of this oscillation have been observed systematically and reported in detail in references 12 and 13. Data were taken which confirmed the functional dependence of frequency on the square root of the product $\hat{n}_e\hat{n}$ given by equation (24). A log-log plot of experimental data for deuterium gas, taken from reference 13, is shown in figure 10. The observed frequencies for this gas ranged from 340 to 50 500 hertz.

The observed neutral density was based on the vacuum gage reading. Relative values of the electron density were measured by a technique based on analysis of the retarding potential curves from a gridded electrostatic analyzer, discussed in reference 22. The best-fitting straight line of slope 0.5 is drawn through the data points in figure 10. The good agreement of this slope with the data, over five orders of magnitude in the product $\hat{n}_e\hat{n}$, confirms the square root dependence of ν on the product $\hat{n}_e\hat{n}$ given by equation (24).

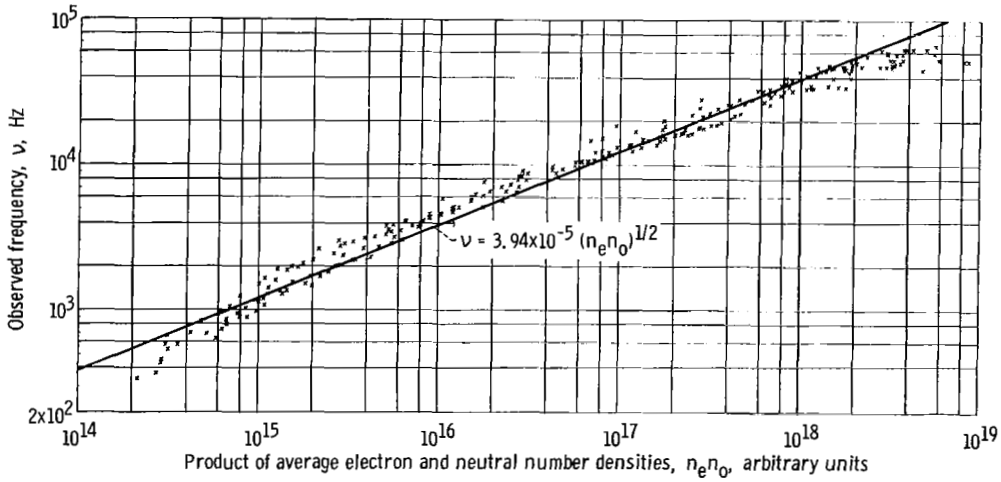

Figure 10. - Observed frequency of continuity equation oscillation as function of average electron and neutral number density product, in arbitrary units, for 247 data points taken with deuterium gas (ref. 13). The best-fitting straight line of slope 1/2 is drawn through data, confirming dependence of ν on $(\hat{n}_e\hat{n})^{1/2}$.

Frequency Stability of Oscillation

One of the outstanding characteristics of the pulsars is long-term frequency stability, with long-term variations being no more than one part in 10^6 or 10^7 during 6 months or more.

An experiment was made to assess the frequency stability of the laboratory plasma, and confirm that any drift observed could be accounted for by the observed drift in or measurement uncertainty of the electron and neutral number density of the plasma. Individual pulses of electrons reaching the collector plate of a multigrid electrostatic analyzer were counted for 30 seconds. A schematic diagram of the instrumentation is shown in figure 11. One such 30-second measurement of the frequency was taken at 5 minute intervals over a 200 minute experimental run. Special precautions were taken to keep the experimental conditions as constant as the nature and limitations of the apparatus would permit.

The result of this frequency stability run is shown in figure 12. During this 200 minute run, the frequency varied by ±3 percent about its mean value. This variation is easily accounted for by the ±2.7 percent variations that were measured in the neutral pressure, and the ±13 percent variations that were measured in the electron density. These apparent fluctuations in electron and neutral number density were probably largly due to imprecision of the measuring techniques used, amounting to ±2 percent for relative measurements of the neutral density, and as much as ±20 percent for relative measurements of the electron density (ref. 22). The operating conditions could not be controlled sufficiently to test the ultimate frequency stabiliby of the oscillation. It is interesting to note, however, that the few percent variation of the 28 kilohertz frequency shown in figure 12 for 200 minutes implies that the frequency did not change by more than a few percent over about 3.3×10^8 individual pulses. This would imply a similar degree of frequency stability over about 10 years in a 1 second pulsar.

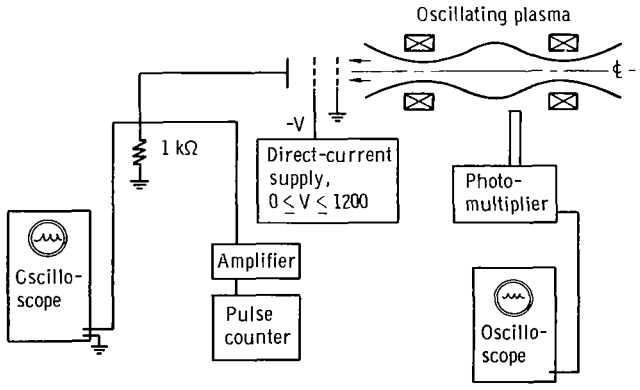

Figure 11. - Schematic drawing of instrumentation used to study waveforms of pulsed electron output and light intensity. Photomultiplier integrated light intensity across diameter of discharge.

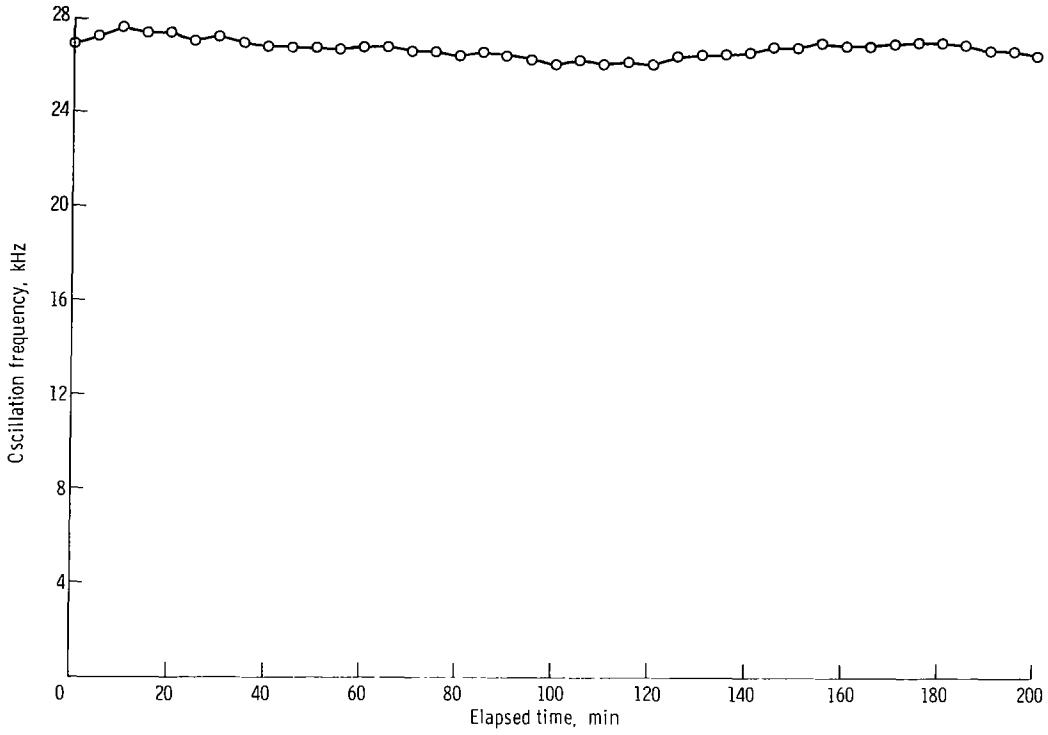

Figure 12. - Observed continuity-equation oscillation frequency as function of time, for a 200-minute experimental run. Variation of frequency was ±3 percent of average value, which was within limits to which electron and neutral number density could be controlled.

Experimental Waveform of $n_e(t)$

The pulsar waveforms shown on figures 1 and 2 are of radio frequency emission, and the fine structure therein may be ascribed to the mechanism by which the RF emission is produced. Nonetheless, it is of some interest to measure the time-dependent electron density in the discharge, and see what similarities and differences exist with respect to the waveforms of the pulsars shown in figures 1 and 2. The waveform of the ion current flowing from discharge was measured by connecting the collector of the energy analyzer shown in figure 11 to ground through a 1 kΩ resistor. The voltage drop across this resistor was then displayed on an oscilloscope, and gives a measure of the ion current lost from the discharge. Since the Debye distance was small, the ion and electron currents flowing from the discharge should be equal and in phase. The oscilloscope traces of ion current should be virtually identical with the instantaneous electron and ion density within the discharge, except for a transit-time spreading of the ions with different velocities.

A representative sample of the data showing ion pulses from the discharge is given in figure 13. The specific operating conditions under which each was taken is listed in table I. In each photograph, the time increases from right to left, and the zero level is

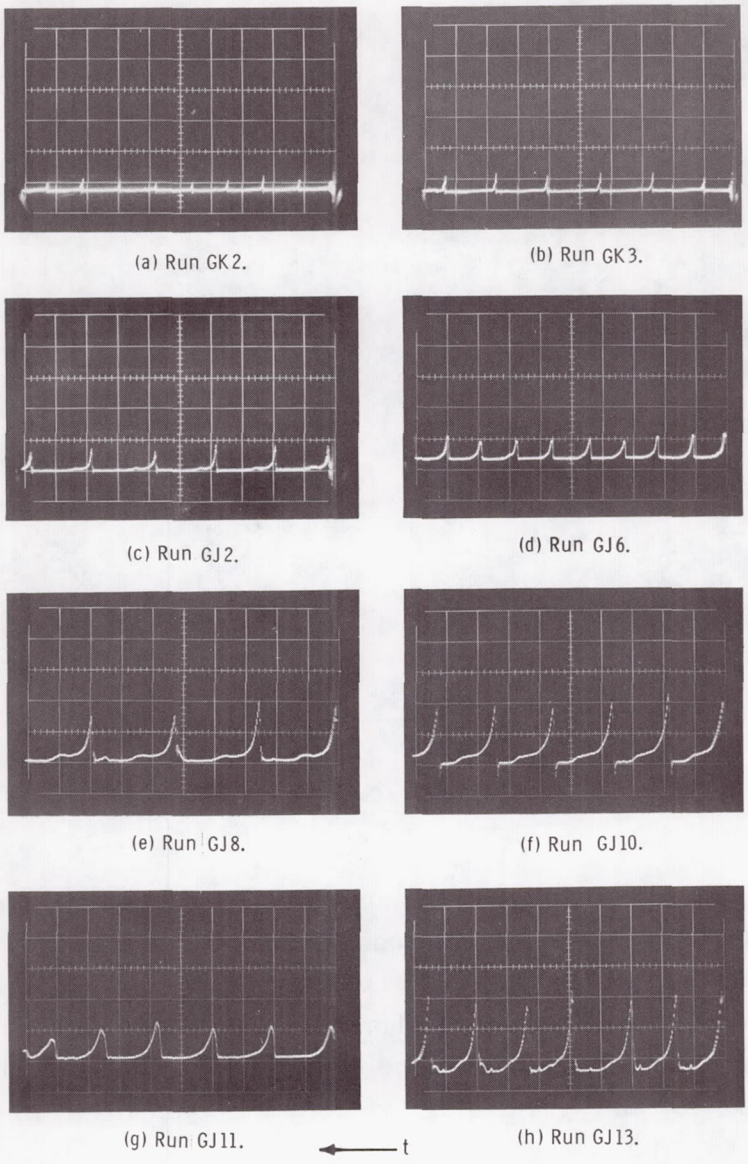

Figure 13. - Experimentally measured waveforms of pulsed electron flux from discharge subject to continuity-equation oscillation. Experimental conditions for each case are listed in table I. All runs shown were with deuterium gas, at a maximum magnetic field of $B_{max} = 1.0$ telsa. Electron number density is proportional to anode current. Zero level is baseline, or lowest excursion, of trace between pulses.

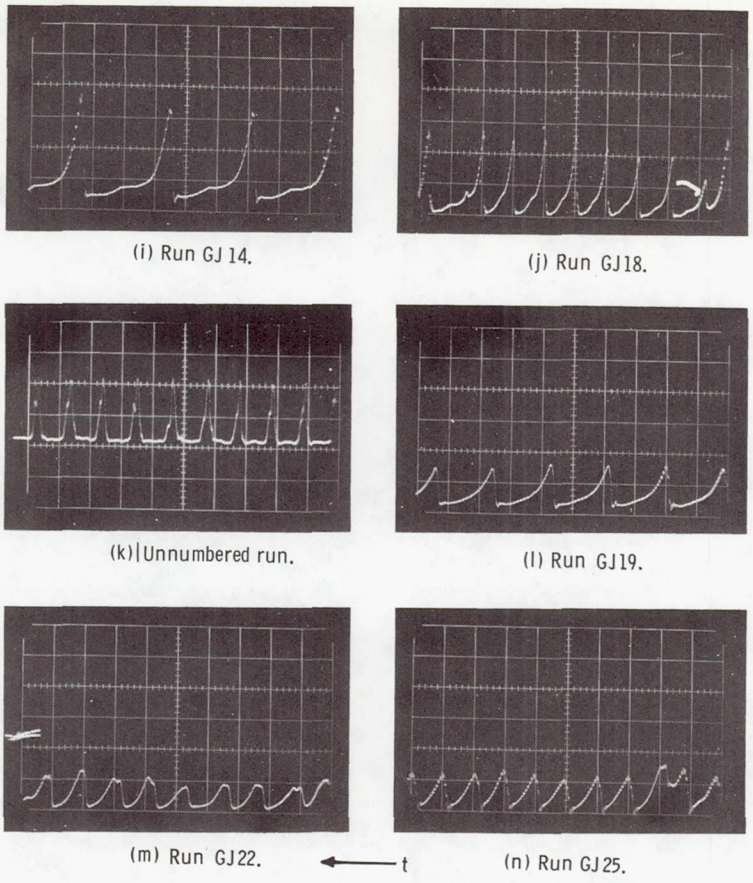

Figure 13. - Concluded.

the baseline between pulses. The electron number density is proportional to the anode voltage shown in table I for a fixed neutral number density. In general, the pulses become broader and less regular as the neutral density was increased. The "tail" following the initial sharp pulse is not primarily due to a velocity selection effect, in which slower particles arrive after the faster. The transit time from the center of the discharge to the analyzer for an ion of average velocity was typically 1/10 the width of these tails.

The light output was monitored with a type IP28 photomultiplier, the output of which was displayed on an oscilloscope. A representative sample of these records of light output is shown in figure 14. In these traces, the zero level is at the bottom of the graticule and time increases from right to left.

The maxima in the light output was synchronous with the pulse of ions emitted from the discharge. The light and ion and electron efflux pulsations had the same frequency and were in phase.

TABLE I. - OPERATING CONDITIONS FOR WAVEFORMS OF

$n_e(t)$ IN FIGURE 13

Waveform	Run	Indicated tank pressure, torr	Direct-current anode voltage, kV	Average anode current, mA	y-axis scale, mV per major division	x-axis scale, μsec per major division
13(a)	GK2	2.45×10^{-6}	10	3	1.0	200
13(b)	GK3	2.45	15	4.5		200
13(c)	GJ2	4.75	10	4		50
13(d)	GJ6	8.1	5	2.5		50
13(e)	GJ8	8.1	15	8.5		20
13(f)	GJ10	8.1	25	14		↓
13(g)	GJ11	1.2×10^{-5}	5	3.5		
13(h)	GJ13	1.2	15	11.5		
13(i)	GJ14	1.2	20	15	↓	10
13(j)	GJ18	1.65	15	17	2.0	20
13(k)	----	2.2	10	14	2.0	20
13(l)	GJ19	1.65	20	21	2.0	10
13(m)	GJ22	2.6	10	24	5.0	10
13(n)	GJ25	2.6	25	46	5.0	10

TABLE II. - OPERATING CONDITIONS FOR WAVEFORMS OF LIGHT

INTENSITY IN FIGURE 14

Waveform	Run	Indicated tank pressure, torr	Direct-current anode voltage, kV	Average anode current, mA	y-axis scale, mV per major division	x-axis scale, μsec per major division	Gas
14(a)	Gi9	2.6×10^{-6}	4	1.3	10	100	He
14(b)	Gi8	2.65	5	1.6	10	100	↓
14(c)	Gi6	2.8	10	3.3	20	↓	
14(d)	Gi2	3.1	20	7.1	100		↓
14(e)	CR10	7.4	5	3	200		D_2
14(f)	CR12	7.4	8	5	200	↓	D_2

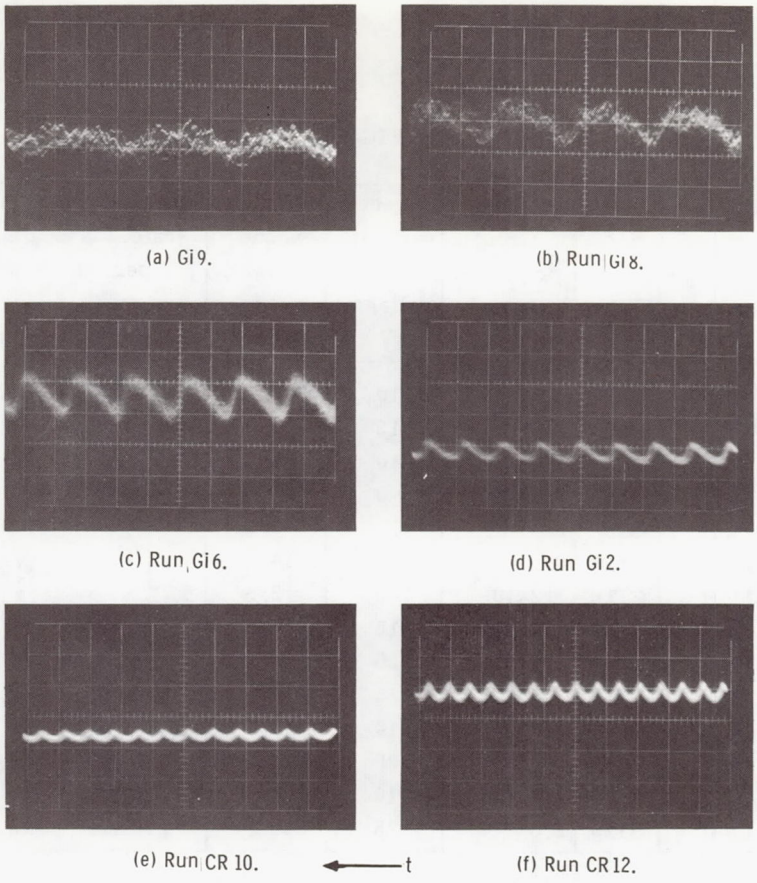

Figure 14. - Light output of discharge for experimental conditions given in table II. Zero level is the bottom of graticule.

QUANTITATIVE ASPECTS OF ASTROPHYSICAL APPLICATIONS

Application to Interstellar H-I and H-II Regions

One possible astrophysical application of equations (3) and (4) is the behavior of interstellar H-I and H-II regions, in which there exists a population of electrons sufficiently energetic to ionize any neutral hydrogen that may be present. The periodic fluctuations in electron density that would arise from this mechanism may be observable indirectly as long-term oscillation of point radio sources, or periodic fluctuations in the angle of rotation of polarized radio waves from a background radio source. If the periodically fluctuating electron population is increased greatly in energy by interstellar electric fields or plasma turbulence, then periodically fluctuating radio frequency emission may result from bremsstrahlung or cyclotron radiation mechanisms.

The expected period of such oscillations in the interstellar medium is approximately given by equation (27).

$$T \approx \frac{2\pi}{\sqrt{\hat{n}_e \hat{n}}\ \langle \sigma v \rangle_{ne}} \tag{25}$$

The reaction rate parameter $\langle \sigma v \rangle_{ne}$ for atomic hydrogen has a maximum value at 100 electron volts electron energy given by

$$\langle \sigma v \rangle_{ne\ max} \approx 3 \times 10^{-8}\ cm^3/sec \tag{26}$$

(ref. 15, fig. 25). The accepted maximum value of the interstellar neutral hydrogen density is $\hat{n} \approx 1$ atom per cubic centimeter, and a charged particle number density of $\hat{n}_e \times 0.5$ electron per cubic centimeter (ref. 23, p. 254). These values, when substituted into equation (25) with the reaction rate parameter in expression (26), yield a period of

$$T \approx \frac{2\pi \sqrt{2}}{3 \times 10^{-8}} \approx 10\ years \tag{27}$$

If the electron population were cooler or substantially hotter than 100 electron volts, $\langle \sigma v \rangle_{ne}$ would be smaller than that given by equation (26), and the period would be larger than indicated by equation (27). These long-period fluctuations in the density of the interstellar electron number density may give rise to scintillations in the strength and polarization of radiation from radio stars. Such scintillations have not been observed, but this may be because radio-astronomical data have not been taken for a sufficiently long time.

If the oscillating region had a higher electron and neutral density, the oscillation periods may be on the order of months. Oscillations due to this continuity-equation mechanism may be responsible for the quasi-periodic fluctuations, with characteristic times of the order of months, that have been observed in the X-ray emission of certain astronomical objects (refs. 24 and 25).

Application to Planetary Atmospheres

From the examples studied to date, it appears that the upper reaches of planetary atmospheres contain both neutral and charged particles. The charged particle density is much enhanced if the planet in question has a dipole magnetic field strong enough to trap such particles.

It is shown in appendix C that in-phase oscillations with a single frequency are probable if the product $\hat{n}_e\hat{n}$ is constant over a significant region in the planetary atmosphere. A more usual situation is one in which $\hat{n}_e\hat{n}$ varies with height. Each height probably would oscillate in electron number density with a characteristic frequency of its own, and the net result would then be a broad spectrum of electron number density oscillation frequencies.

The presence of a planetary magnetic field greatly enhances the likelihood of the oscillations of $n_e(t)$ having observable effects. The periodic loading of the geomagnetic field lines with electrons may, for example, result in observable low-frequency periodic fluctuations in the strength of the magnetic field at the planetary surface. Such low-frequency oscillations - called "geomagnetic micropulsations" - are observed on the surface of the earth (refs. 26 to 28). Their origin is obscure, and they may be caused by continuity-equation oscillations in the electron number density of the magnetosphere.

If the electron number density is oscillating with a single frequency over a significant vertical distance, if a strong geomagnetic field is present, and if the electrons are raised quickly to higher energies by turbulent heating or some other process, one might then expect to find radio-frequency emission from the trapped electrons, modulated by the continuity-equation frequency. It is very doubtful, however, whether such planetary "pulsars" have enough energy available for RF emission to be detected outside their own solar system.

It is of interest to run a quantitative check and see whether the electron and neutral number densities in the earth's exosphere are consistent with the geomagnetic micropulsation frequencies actually observed. It is known that there is no extensive region in the earth's magnetosphere in which the product $\hat{n}_e\hat{n}$ is constant; it decreases monotonically with radius above an altitude of 100 kilometers. One would then expect a continuous distribution (spectrum) of frequencies. Such a continuous distribution is characteristic of the geomagnetic micropulsations. The period of the geomagnetic micropulsations, if given by equation (25), is inversely proportional to $(\hat{n}_e\hat{n})^{1/2}$. This implies that the period of the pulsations ought to be relatively long during the quiet times of solar sunspot minimum, when $\hat{n}_e$ is low. Near sunspot maximum, when $\hat{n}_e$ is enhanced by large factors over the values characteristic of sunspot minimum, one would expect the geomagnetic micropulsation period to be shorter. Such a trend of shorter period micropulsations with increasing solar activity (and hence indirectly with increasing $\hat{n}_e$ in the magnetosphere) has been observed (ref. 26).

In reference 28 it is reported that geomagnetic micropulsations were observed simultaneously at conjugate points in the geomagnetic field; observations of in-phase oscillation over distances as great as 1000 kilometers are quite common (ref. 28). This suggests that, if the continuity-equation oscillation is responsible for the oscillations, they must originate at a sufficiently high altitude such that the electron mean free path is about

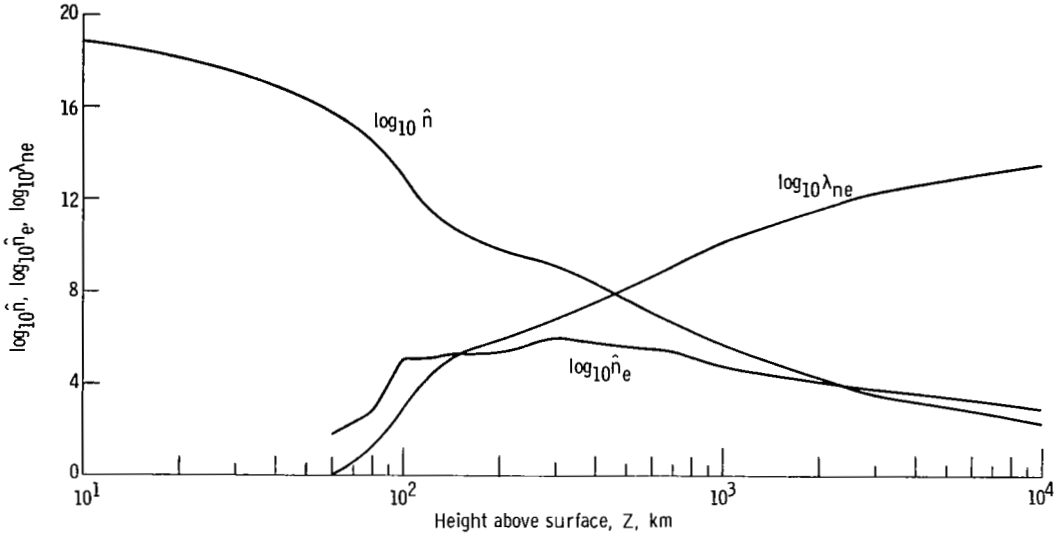

Figure 15. - Variation of electron density, neutral density, and mean free path of electrons as function of height above surface of Earth. Data were taken from reference 23, electron oscillation cross section was taken as 1.4×10^{-16} square centimeter.

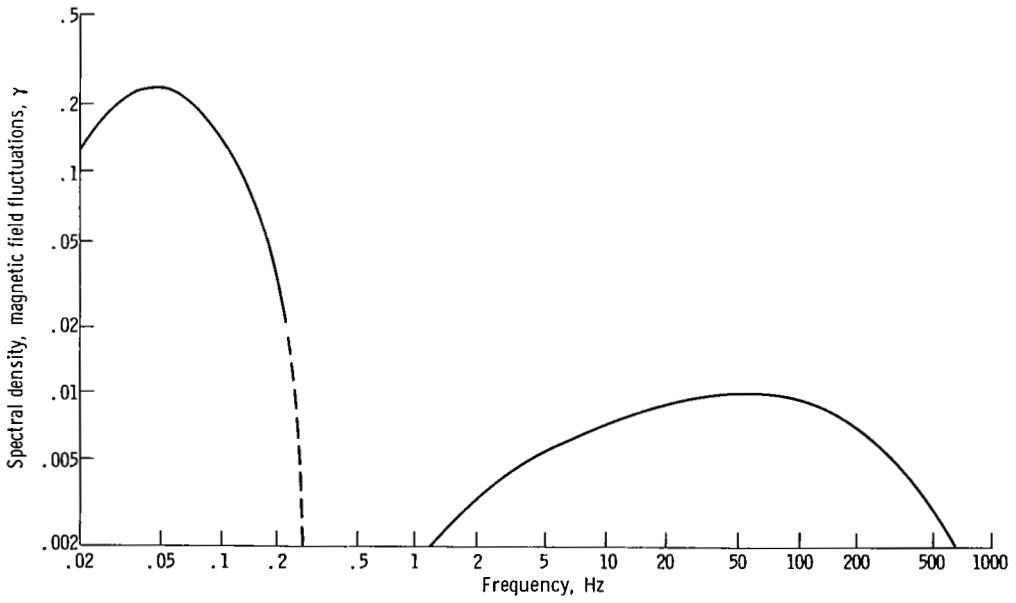

Figure 16. - Spectrum of geomagnetic micropulsations, magnetic field amplitude as a function of frequency. From reference 27.

10^3 kilometers. On figure 15 is shown a log-log graph of the electron mean free path, and electron and neutral number densities as a function of height above the earth's surface. The electron mean free path is 10^3 kilometers at an altitude of about 500 kilometers. At this altitude, the electron number density is approximately 4×10^5 per cubic centimeter, and the neutral density is approximately 5×10^7 per cubic centimeter. The dominant species at an altitude of 500 kilometers is atomic oxygen (ref. 29), whose maximum ionization rate parameter is given by Lotz (ref. 15, fig. 32) as $\langle\sigma v\rangle_{ne,\,max} \approx 10^{-7}$ cubic centimeter per second. Substituting these values into equation (32) we obtain a continuity-equation period of

$$T \approx \frac{2\pi}{10^{-7}(4\times10^5\times5\times10^7)^{1/2}} \approx 14 \text{ sec} \tag{28}$$

This frequency is quite close to the maximum spectral amplitude of about 0.05 hertz (period 20 seconds) actually observed in the geomagnetic micropulsations, a spectrum of which is shown in figure 16 (ref. 27).

Application to Stellar Atmospheres

The preceding discussion of continuity-equation oscillations in planetary atmospheres is relevant in its qualitative features to stellar atmospheres, with two important differences: The first difference is that near a stellar surface, large amounts of energy are available for conversion to radio-frequency power. Enough energy is available so that if a conversion process is active over an entire stellar surface, even a very inefficient process can radiate enough power to be detected at interstellar distances. The second difference is that if pulsars are to be explained in terms of the periodic generation of electrons by the continuity-equation oscillation mechanism, then there must exist a large region in the stellar atmosphere over which the product $\hat{n}_e\hat{n}$ is constant.

The decrease of neutral density with height above a stellar surface may be approximated by the isothermal law of atmospheres,

$$n(Z) = n_1 e^{-Z/H_o} \tag{29}$$

The requirement of in-phase oscillations of a single frequency then requires that $n(Z)n_e(Z)$ be constant, or that $n_e(Z)$ have the functional form

$$n_e(Z) \approx n_{e,\,max} e^{+Z/H_e} \tag{30}$$

where $H_e=H_o$ and the electron number density increases with distance above the stellar surface. This increasing n_e could be the base of a stellar magnetosphere, in which the electron population increased exponentially as one moved from the neutral atmosphere into the base of the stellar "Van Allen Belts." Such a stellar magnetosphere would imply a strong magnetic field, which would promote radio-frequency emission from energetic electrons.

Substituting equations (29) and (30) into equation (25), we have an expression for the period of a pulsar,

$$T = \frac{2\pi}{(\hat{n}_e \hat{n})^{1/2} \langle \sigma v \rangle_{ne}} \approx \frac{2.1 \times 10^8}{(\hat{n}_e \hat{n})^{1/2}} \text{ sec} \tag{31}$$

where the maximum ionization rate parameter for hydrogen, in equation (26), has been used. For the pulsar CP1919, with a period of 1.337 seconds, equation (31) implies a product of electron and neutral number density.

$$\hat{n}_e \hat{n} \approx 2.46 \times 10^{16} / \text{cm}^6 \tag{32}$$

This appears to be a reasonable number density product to be found in a stellar atmosphere (ref. 23, p. 161).

If the continuity-equation oscillation is confirmed as governing the frequency of pulsars, a measurement of their period would then yield information about the product of electron and neutral number densities in a large region of the stellar atmosphere.

It may be objected that the great stability of the pulsar frequency is inconsistent with the continuity-equation oscillation, since the electron and neutral number densities may be expected to fluctuate significantly in a typical stellar atmosphere. While this is true locally, the expression for n(Z) given in equation (29) involves only quantities whose values averaged over an entire stellar surface (n_1, H_o) would be expected to vary only on an astronomical time scale. Temporal constancy of the electron number density is understandable on the hypothesis of a very strong dipole magnetic field, which may average the stellar magnetospheric production and loss processes over the entire stellar surface, and over trapping times much larger than a pulsar period. Such an averaging process should be effective if the star is not subject to the equivalent of our 22-year solar sunspot cycle, or if the number of charged particles stored in the stellar Van Allen Belts is much larger

than the number gained or lost over the length of time during which the oscillation period is observed to be constant.

DISCUSSION

Synchronization of Pulsating Region

The pulsar waveforms shown on figures 1 and 2 have rise times as short as one millisecond. It is usually argued that this rise time, when multiplied by the speed of light, places an upper bound on the size of the oscillating region. This limit results from the implicit assumption that a triggering signal must propagate throughout the volume of the oscillating region during the fast rise portion of the waveform.

It is a highly significant fact that, if the continuity-equation oscillation is responsible, such a triggering signal is not required for the production of synchronized pulses, and the size of the pulsating object is not limited to the product of the rise time and the speed of light. To see how this may be so, consider a "thought experiment" performed with two identical clocks, synchronized to one part in 10^8. Suppose that these two clocks emit synchronized pulses every second, with an initial rise time of 10^{-6} seconds. If these two clocks are placed on the opposite limbs of a star separated by a distance of (say) 1 light-second, an observer in an external stellar system will see the situation shown in figure 17. The observer will note the 1 microsecond rise time of the signals, and, being unaware of the situation, will incorrectly conclude that the pulsating object is no more than 300 meters in diameter, whereas in fact the clocks are 1 light second, or 300 000 kilometers apart.

It is important to realize that, if the ionization rate parameters $\langle \sigma v \rangle_{ne}$ are the same, two spatially separated regions of partially ionized gas will behave like two independent clocks whose frequency of oscillation is determined only by the product $\hat{n}_e \hat{n}$. An examination of the laboratory data presented in figure 13 shows that the rise time of the electron number density can be as small as 1 microsecond in this laboratory plasma, so the continuity-equation oscillation mechanism is capable of producing pulses of electrons with very short initial rise times.

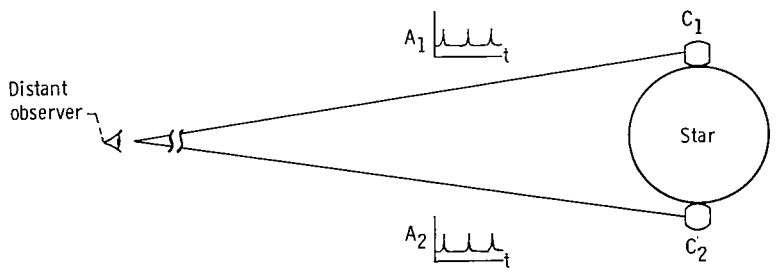

Figure 17. - Observer looking at two synchronized clocks separated by 1 light second.

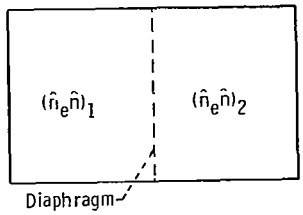

Figure 18. - Schematic of two adjacent volumes in region subject to continuity-equation oscillation. If diaphragm is removed at time t = 0, mixing will occur, and products of electron and neutral number densities will become the same. Thus, both regions will oscillate with the same frequency. Phases of oscillation can become synchronized by mechanism discussed in text.

One can understand how adjacent regions can assume the same frequency and phase by considering the schematic arrangement in figure 18. Suppose that initially the two adjacent regions are isolated and have different values of $\hat{n}_e\hat{n}$. If the diaphragm is removed at time $t = 0$ any transport process such as collisions, turbulence, ionospheric winds, etc. will cause a mixing of the electron and neutral number densities in adjacent regions. This will lend to both regions having the same values of $\hat{n}_e\hat{n}$ and the same oscillation frequency.

It is also understandable that the two regions should have the same phase, as well as the same frequency. If the right-hand region pulses slightly in advance of the left-hand region, the particles which are lost from the right-hand region will pass over into the left-hand region and trigger it to pulse before it would have done so without an outside disturbance. The particles which move from one region to surrounding regions therefore can act as a synchronizing and phase-locking mechanism. One can use an obvious extension of the above argument to show that after an initial period of incoherence and adjustment, a region of very large dimensions may be synchronized, if the product $\hat{n}_e\hat{n}$ is constant throughout the region.

Possible Experimental Checks

Any observations of a pulsar may reveal fine structure in the RF radiation which is consistent with many small regions within the source radiating independently, but with the same modulation frequency. These regions would have been excited by an expanding spherical shell of electrons from the oscillating layer. The small phase differences observed between individual peaks in the fine structure can be attributed to time delays at

the source arising from RF emission at different places and times near the pulsar, or to pulses of electrons originating at different locations within the oscillating region. Fine structure therefore need not be a characteristic of solutions to the continuity equations, but is consistent with probable secondary processes which produce the radiation. The existence of fine structure, recently reported by Craft, et al. (ref. 7), is consistent with this model. According to Craft, et al. (ref. 7), if the pulses shown on figures 1 and 2 are examined under high temporal resolution, they resolve themselves into hundreds or thousands of individual sharply peaked pulses.

When the periods are comparable or greater than the electron transit time across the oscillating region (as is the case with geomagnetic micropulsations), one would then expect the source to behave as a single oscillating region, with no fine structure to the pulses.

An experimental check can be provided by an observation of light output. The reaction rate parameter $\langle \sigma v \rangle_{ex}$ for excitation of atomic hydrogen is of the same order of magnitude as the ionization rate parameter $\langle \sigma v \rangle_{ne}$, and one would therefore expect oscillations in the electron number density to be accompanied by in-phase oscillations of the light. This was, of course, observed in the laboratory experiment discussed above. The peak-to-peak fluctuation in visible light will be quite small by comparison with the radiant intensity of a stellar surface, unless the star in question is extremely efficient in converting its total energy output into energetic charged particles. One would, therefore, not expect to be able to observe fluctuatuons in light output when the oscillating source is in a stellar atmosphere. If such oscillations were observed, they should be of the same frequency and phase as the fluctuations of electron number density. If observations are confirmed of fluctuatuons in light output with a frequency different from the pulsar frequency, this would tend to rule out the continuity-equation oscillation mechanism, unless complicated additional physical mechanisms are invoked.

When there is no bright background source behind the pulsating region, it may then be possible to detect long-period fluctuations in the light output of the pulsating region which would be in phase with the fluctuations in electron number density. Such an observation does, of course, presuppose coherent oscillations and an adequate optical depth of gas.

The pulsars observed thus far all seem to posess characteristic sharp, narrow peaks separated by broad, flat minima, whose minimum values are at or below the radio-frequency noise level. If the pulses are due to the continuity-equation oscillation, then this waveform suggests that η_e of equation (20) has either values $\eta_e >> 1.0$, or $\eta_e << 1.0$ (ref. 11). One might expect to find, sooner or later, a pulsar for which $\eta_e \approx 1.0$. The radio-frequency waveform in this case would be expected to have a sinusoidal modulation, and a constant, nonzero minimum level of radio-frequency emission, well above the background noise level.

If independent means are available to measure the electron and/or neutral number densities, one should observe a correlation between changes in the oscillation period and changes in the products $\hat{n}_e\hat{n}$. If the period is constant (as it appears to be in pulsars), then this product should be observed to remain constant.

CONCLUSIONS

The continuity-equation oscillation provides a simple, straightforward physical mechanism by which electrons can be produced in periodic pulses by a partially ionized plasma.

Arguments have been put forward to show that this mechanism is quantitatively and qualitatively consistent with such periodic astrophysical phenomena as pulsars, geomagnetic micropulsations, and periodic variations in the electron number density of interstellar H-I or H-II regions.

The continuity equations have been derived for a grossly uniform spherical mass of gas, and for a planetary or stellar atmosphere in which the neutral and charged particle number density vary with height above the surface. It has been shown that if the ionization mean free paths are longer than the smallest dimension of the region, an oscillation in electron number density will occur which arises from transit time delays associated with the passage of neutrals across the ionized gas. These transit time delays are significant in that they prevent a detailed balance between the production and loss terms of the continuity equations.

If the ionization mean free paths are long compared to the characteristic dimensions of the ionized gas, and if energetic electrons are available to cause ionization, then periodic oscillations in electron number density are a natural outcome of the operation of the continuity equations. Such oscillations have been observed over more than five orders of magnitude in the product $\hat{n}_e\hat{n}$ in the laboratory, and frequencies as low as 87 hertz have been experimentally observed. Much lower frequencies would be expected in the lower electron and neutral number densities characteristic of astrophysical conditions.

Lewis Research Center,
National Aeronautics and Space Administration,
Cleveland, Ohio October 20, 1968,
129-02-08-06-22.

APPENDIX A

SYMBOLS

[All quantities are in SI units unless noted otherwise]

A_i	coefficients of terms in charged particle continuity equation
C_i	coefficients of terms in neutral particle continuity equation
$G(\eta, \delta)$	frequency reduction parameter
H_e	scale height of electron number density, assumed to increase exponentially with height
H_o	scale height of neutral, isothermal atmosphere
L	characteristic dimension of oscillating region
n	neutral density
$\hat{n}$	time and space averaged value of neutral particle density
$\tilde{n}$	time averaged neutral number density, in region where n is virtually constant in space
n_e	electron density
$\hat{n}_e$	time and space averaged electron number density
$\tilde{n}_e$	time averaged electron number density, in region where n_e is virtually constant in space
$n_{e,\max}$	time-dependent electron number density at top of oscillating region in a planetary or stellar atmosphere
n_{eo}	initial extremal value of $n_e(t)$ at $t = 0$
n_o	surrounding neutral gas density
n_1	neutral number density at Z_{min}
$\tilde{n}_1$	time averaged neutral number density at Z_{min}
R	radius of spherical oscillating region
r	radial coordinate
T	period of oscillation, sec
t	time
t_d	transit time of downward-moving neutral particle

t_{ne}	mean free time between electron-neutral collisions
t_o	transit time of neutral across oscillating region
t_{oe}	transit time of electrons across characteristic discharge dimension
t_{or}	transit time across radius R of spherical region
t_u	transit time of upward-moving neutral particle
V_e	electron energy, eV
v	neutral velocity
v_e	electron velocity
x	dimensionless neutral density, defined by eq. (17)
y	dimensionless electron density, defined by eq. (18)
Z	height above surface of a star or planet
Z_{max}	upper boundary of oscillating region in a planetary or stellar atmosphere
Z_{min}	lower boundary of oscillating region in a planetary or stellar atmosphere
β	argument of electron number density variation, defined by eq. (E3)
β_o	phase angle resulting from transit time across discharge, defined by eq. (E4)
δ	extremal fraction of ionization
$\delta n(t)$	small time-dependent perturbation of neutral density
$\hat{\epsilon}$	space and time averaged attenuation coefficient of neutrals, averaged over prior path in discharge, defined by eq. (B4)
$\tilde{\epsilon}_d$	time averaged attenuation coefficient of downward-moving particles
$\tilde{\epsilon}_u$	time averaged attenuation coefficient of upward-moving particles
η_e	electron amplitude index used in exact numerical solutions of eqs. (22) and (23), defined by eq. (20)
η_s	amplitude index used in small-amplitude solutions
λ_{ne}	mean free path of a neutral for an ionizing collision
ν	frequency, Hz
φ_n	net neutral flux at a point
φ_{ne}	net flux of electrons through a point
φ_T	total neutral particle flux through a point
φ_u	flux of upward-moving neutral particles

ψ dimensionless attenuation coefficient, in spherical region, defined by eq. (B5)

ψ_d dimensionless attenuation coefficient of downward-moving particles, given by eq. (C9)

ψ_u dimensionless attenuation coefficient of upward-moving particles, defined by eq. (C7)

ρ path length of neutral in spherical oscillating region

$\langle \sigma v \rangle_{ne}$ ionization rate parameter, for ionization of neutrals by electron impact

τ dimensionless time, defined by eq. (21)

θ polar angle in spherical coordinates

APPENDIX B

DERIVATION OF CONTINUITY EQUATIONS IN A SPHERICALLY SYMMETRIC ISOLATED REGION OF PARTIALLY IONIZED GAS

One possible application of the continuity-equation oscillation mechanism is to partially ionized interstellar H-I or H-II regions. The spherically symmetric mass of gas shown in figure 19 will be adopted as a model of such a region. Both the electron number density and neutral density are assumed uniform over the region, except for the very small spatial and temporal perturbations caused by the ionization process itself. The electrons may be confined to the region of interest, or may also exist in the region outside the discharge. The electrons could, for example, be confined to the region of interest by a local magnetic field perturbation in the form of a magnetic bottle. For this analysis, it is assumed that the neutral atoms are isotropic in velocity space, and monoenergetic.

Consider the net flux of particles at a position r from the center of a spherical region of radius R. The differential flux of neutrals reaching position r has been attenuated by an amount proportional to the path length ρ in the region. If the ionization mean free path of a neutral is much larger than the characteristic dimension of the region, $L \approx 2R$, the radial flux through a unit area at the point r with a normal pointing along r is

$$d\varphi_n(\theta) = \frac{1}{2} n_o v e^{-\tilde{\epsilon}\rho} \cos\theta \sin\theta \, d\theta \tag{B1}$$

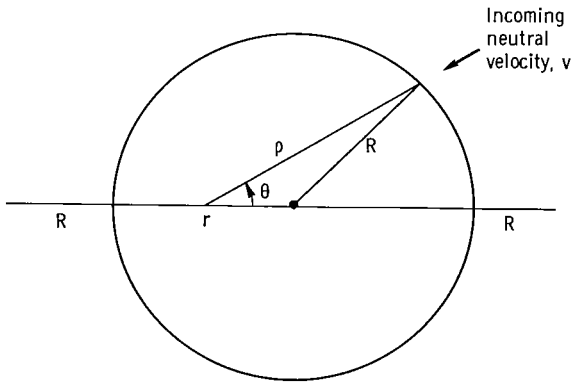

Figure 19. - Geometry of spherical oscillating region, assumed to be surrounded by neutral gas having an isotropic, monoenergetic velocity distribution. Only neutral particles whose velocity vectors have a polar angle θ will pass through point r.

where one has used spherical symmetry to integrate over the azimuthal angle. The region is assumed surrounded by neutral gas of density n_o. This net flux is zero for an isotropic velocity distribution. The instantaneous value of the absorbtion parameter ϵ is the inverse of the electron-neutral mean free path,

$$\epsilon = \frac{1}{\lambda_{ne}} = \frac{n_e(t')\langle \sigma v \rangle_{ne}}{v} \tag{B2}$$

This must be averaged over all previous times during which a particle passing through the point r could have been in the discharge, and hence subject to ionization. The maximum length of time a neutral particle can be in the discharge before reaching the point r is

$$t_o = \frac{\rho}{v} \tag{B3}$$

The average absorbtion coefficient is found by integration over all times from $t-t_o$ to t,

$$\tilde{\epsilon} = \frac{1}{t_o} \int_{t-t_o}^{t} \frac{n_e(t')\langle \sigma v \rangle_{ne}}{v} dt' = \frac{\langle \sigma v \rangle_{ne}}{\rho} \int_{t-t_o}^{t} n_e(t')dt' \tag{B4}$$

since $\langle \sigma v \rangle_{ne}$ and v are not functions of time by hypothesis. It is helpful to define the attenuation coefficient

$$\psi \equiv \tilde{\epsilon}\rho = \langle \sigma v \rangle_{ne} \int_{t-t_o}^{t} n_e(t')dt' \tag{B5}$$

The differential flux of equation (B1) may then be written

$$d\varphi_n(\theta) = \frac{1}{2} n_o v e^{-\psi} \cos\theta \sin\theta \, d\theta \tag{B6}$$

It should be noted that ψ is a function of both r and θ, through its dependence on ρ in the lower limit t_o. The net radial flux at position r is given by integrating over all possible polar angles,

$$\varphi_n(r) = \frac{1}{2} n_o v \int_o^{\pi} e^{-\psi} \sin\theta \cos\theta \, d\theta = n_o v_d \tag{B7}$$

where v_d is the macroscopic drift velocity of neutrals into an elemental volume around the point r.

The neutral particle continuity equation can be written

$$\dot{n} = -\nabla \cdot \varphi_n - n n_e \langle \sigma v \rangle_{ne} \tag{B8}$$

The divergence term in this equation can be written in spherical coordinates, by using equation (B7)

$$-\nabla \cdot \varphi_n = -\frac{1}{r^2} \frac{d}{dr} \left(\frac{r^2 n_o v}{2} \int_0^{\pi} e^{-\psi} \sin\theta \cos\theta \, d\theta \right)$$

$$= -\frac{n_o v}{r} \int_0^{\pi} e^{-\psi} \cos\theta \sin\theta \, d\theta + \frac{n_o v}{2} \int_0^{\pi} \frac{d\psi}{dr} e^{-\psi} \sin\theta \cos\theta \, d\theta \tag{B9}$$

The derivative within the integral sign in equation (B9) may be obtained by using equations (B3) and (B5) which yield

$$\frac{d\psi}{dr} = \frac{n_e (t - t_o) \langle \sigma v \rangle_{ne}}{v} \frac{d\rho}{dr} \tag{B10}$$

By applying the law of cosines to figure 19 one can obtain a relation between ρ, r, and $\cos\theta$, as follows:

$$\rho^2 = R^2 - r^2 + 2r\rho \cos\theta \tag{B11}$$

differentiating this with respect to r, one obtains

$$\frac{d\rho}{dr} = \frac{\rho \cos\theta - r}{\rho - r \cos\theta} \tag{B12}$$

Substituting equations (B10) and (B12) into equation (B9) one obtains for the divergence term

$$-\nabla \cdot \varphi_n = -\frac{n_o v}{r} \int_0^{\pi} e^{-\psi} \cos\theta \sin\theta \, d\theta$$

$$+ \frac{n_o \langle \sigma v \rangle_{ne}}{2} \int_0^{\pi} n_e(t-t_o) \frac{(\rho \cos\theta - r)}{(\rho - r\cos\theta)} e^{-\psi} \cos\theta \sin\theta \, d\theta \qquad \text{(B13)}$$

To simplify the analytical and physical aspects of the problem, we specialize to the position $r = 0$ at which ψ is no longer a function of θ, and equation (B3) becomes

$$t_o = \frac{R}{v} \qquad \text{(B14)}$$

By evaluating the second term in equation (B13) at $r = 0$, and applying l' Hôspital's rule to the first term, one obtains the value of the divergence term at the center of the spherical mass of gas,

$$-\nabla \cdot \varphi_n = n_o n_e(t-t_o) \langle \sigma v \rangle_{ne} e^{-\psi} \qquad \text{(B15)}$$

It is now possible to use a calculation of the total flux at $r = 0$ to calculate the time-dependent flux there. The total flux may be written by analogy with equation (B7)

$$\varphi_T(0, t) = n(0, t)v = n_o v e^{-\psi} \int_0^{\frac{\pi}{2}} \sin\theta \cos\theta \, d\theta \qquad \text{(B16)}$$

from which it follows that the time-dependent neutral density at the center of the oscillating region may be written

$$n(0, t) = n_o e^{-\psi} \qquad \text{(B17)}$$

Substibuting equations (B15) and (B17) into equation (B8) for the neutral particle continuity equation yields

$$\dot{n} = n \langle \sigma v \rangle_{ne} \left[n_e(t-t_o) - n_e(t) \right] \qquad \text{(B18)}$$

It is clear that $\dot{n}$ is not zero because of the time lag represented by the retarded time $t_o = R/v$. In practice, the velocity of the neutrals will not have a constant value v, but will have a Maxwellian spread of energies, all the way down to zero velocity. Since some particles travel with extremely small velocities, these will average the attenuation over one or more periods of oscillation. We can then replace the retarded electron number density $n_e(t-t_o)$ by the time averaged number density $\tilde{n}_e$ to yield

$$\dot{n} = n\langle \sigma v \rangle_{ne} (\tilde{n}_e - n_e) \tag{B19}$$

The validity and limits for which one can replace $n_e(t-t_o)$ with $\tilde{n}_e$ are justified by experimental results discussed in appendix E.

One can obtain the continuity equation for the electrons by an argument virtually identical with that above. The electron continuity equation may be written

$$\dot{n}_e = -\nabla \cdot \varphi_{ne} + n n_e \langle \sigma v \rangle_{ne} \tag{B20}$$

The divergence term can be obtained by replacing $n_e(t) \rightarrow n(t)$, $n(t) \rightarrow n_e(t)$, etc., and realizing that the argument of the exponential $e^{\tilde{\epsilon}\rho}$ in equation (B16) is positive, since the ionization process always results in an excess of electrons in the oscillating region. By following a line of argument like that from equation (B1) to equation (B19) one can show that the electron continuity equation can be written

$$\dot{n}_e = n_e \langle \sigma v \rangle_{ne} \left[n(t) - n(t-t_o) \right] \tag{B21}$$

One can replace the retarded value of $n(t-t_o)$ (with t_o now defined in terms of the electron velocity v_e rather than the neutral velocity v) by appeal to the same arguments cited for the previous case,

$$n(t-t_o) \approx \tilde{n} \tag{B22}$$

so that equation (B21) assumes the symmetrical form

$$\dot{n}_e = n_e \langle \sigma v \rangle_{ne} (n - \tilde{n}) \tag{B23}$$

APPENDIX C

DERIVATION OF CONTINUITY EQUATIONS IN AN OSCILLATING REGION IN A STELLAR OR PLANETARY ATMOSPHERE

In a planetary or stellar atmosphere, the electron and neutral density will be dependent upon the distance above the surface. It is, therefore, necessary to generalize the derivation in appendix B to the case for which n and n_e are functions of position as well as time. A model of such an atmosphere is shown on figure 20. The planetary or stellar surface is located at $Z = 0$. The oscillating region is located between a lower boundary at Z_{min} and an upper boundary at Z_{max}. The neutral density in an isothermal atmosphere may be written

$$n = n_1(t) \exp\left[-\frac{(Z-Z_{min})}{H_o}\right] \tag{C1}$$

where H_o is the scale height of the atmosphere.

It is assumed that the neutral particles which move between $Z_{min} \leq Z \leq Z_{max}$ are monoenergetic with the velocity v, and that half of these neutrals are directed upward, and half in the downward direction. It is assumed that the mean free path of both the electrons and neutral particles in this region are much longer than the vertical dimension of the region itself, so that the probability of a neutral being ionized is much less than unity for a single traversal of the oscillating region.

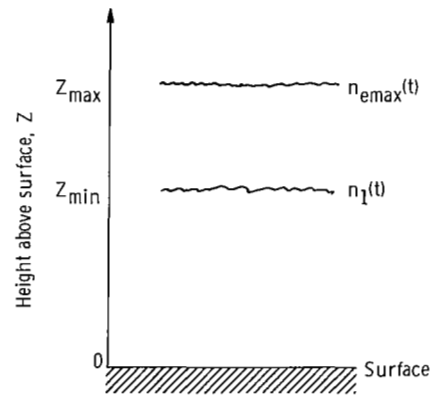

Figure 20. - Geometry of oscillating layer in planetary or stellar atmosphere, confined between heights Z_{min} and Z_{max} above surface.

A downward-moving neutral particle at the height Z will have been in the oscillating region for a transit time t_d given by

$$t_d = \frac{Z_{max} - Z}{v} \tag{C2}$$

and an upward moving particle for a transit time t_u,

$$t_u = \frac{Z - Z_{min}}{v} \tag{C3}$$

The neutral flux will be attenuated exponentially as it moves through the oscillating region. The upward flux may be written

$$\varphi_u = \frac{1}{2} \tilde{n}_1 v \exp\left[- \frac{Z - Z_{min}}{H_o} \right] e^{-\psi_u} \tag{C4}$$

where the upward attenuation factor for neutrals must be written in terms of an average over the time and space varying conditions along the neutral path length. The instantaneous absorbtion coefficient is, by analogy with equation (B2)

$$\epsilon_u = \frac{1}{\lambda_n} = \frac{n_e(Z_u'; t') \langle \sigma v \rangle_{ne}}{v} \tag{C5}$$

If the neutral particle is located at position Z at time t, its position Z_u' at the prior time t' may be written

$$Z_u' = Z - v\,(t - t') \tag{C6}$$

When averaged over the time which the neutral particle has been in the oscillating region, the attenuation coefficient ψ_u is

$$\psi_u = (Z - Z_{min})\, \tilde{\epsilon}_u = \frac{(Z - Z_{min})}{t_u} \int_{t-t_u}^{t} \epsilon_u(Z_u'; t')\, dt' \tag{C7}$$

Substituting equations (C3), (C5), and (C6) into equation (C7) yields

$$\psi_u = \langle \sigma v \rangle_{ne} \int_{t-t_u}^{t} n_e \left[Z - v(t-t'); t' \right] dt' \tag{C8}$$

by a similar argument, the attenuation coefficient for the downward-moving flux is given by

$$\psi_d = \frac{Z_{max} - Z}{t_o} \int_{t-t_d}^{t} \epsilon_d(Z'_d; t')dt' = \langle \sigma v \rangle_{ne} \int_{t-t_d}^{t} n_e \left[Z + v(t-t'); t' \right] dt' \tag{C9}$$

The downward flux can be written in terms of this attenuation coefficient as

$$\varphi_d = \frac{1}{2} \tilde{n}_1 v \exp \left[- \frac{Z - Z_{min}}{H_o} \right] e^{-\psi_d} \tag{C10}$$

The total particle flux at the point Z at time t is

$$\varphi_T = \varphi_u + \varphi_d = n(Z, t)v = \frac{1}{2} \tilde{n}_1 v \exp \left[- \frac{(Z - Z_{min})}{H_o} \right] (e^{-\psi_u} + e^{-\psi_d}) \tag{C11}$$

The neutral density can therefore be written

$$n(Z, t) = \frac{1}{2} \tilde{n}_1 \exp \left[- \frac{(Z - Z_{min})}{H_o} \right] (e^{-\psi_u} + e^{-\psi_d}) \tag{C12}$$

The net flux, with upward moving flux considered positive, is given by

$$\varphi_n = \varphi_u - \varphi_d = \frac{1}{2} n_1 v \exp \left[- \frac{(Z - Z_{min})}{H_o} \right] (e^{-\psi_u} - e^{-\psi_d}) \tag{C13}$$

The neutral particle continuity equation is identical to equation (B8) in this model. The divergence term, however, is

$$-\nabla \cdot \varphi_n = -\frac{d\varphi_n}{dZ} = \frac{1}{2} n_o v \exp\left[-\frac{(Z-Z_{min})}{H_o}\right]\left[\frac{e^{-\psi_u} - e^{-\psi_d}}{H_o} + \frac{d\psi_u}{dZ} e^{-\psi_u} - \frac{d\psi_d}{dZ} e^{-\psi_d}\right] \quad \text{(C14)}$$

Performing the Z-derivatives of equations (C8) and (C14) and (C9), one obtains

$$\frac{d\psi_d}{dZ} = \langle \sigma v \rangle n_e \int_{t-t_d}^{t} \frac{dn_e(Z'_d; t')}{dZ} dt' - \frac{\langle \sigma v \rangle n_e}{v} n_e(Z_{max}; t-t_d) \quad \text{(C15)}$$

and

$$\frac{d\psi_u}{dZ} = \langle \sigma v \rangle n_e \int_{t-t_u}^{t} \frac{dn_e(Z'_u; t')}{dZ} dt' + \frac{\langle \sigma v \rangle n_e}{v} n_e(Z_{min}; t-t_u) \quad \text{(C16)}$$

One cannot proceed further with the derivation without assuming a specific functional form for the altitude variation of n_e. If it is assumed that the electron number density increases exponentially with height,

$$n_e(Z, t) = n_{e,max}(t) \exp\left[-\frac{(Z_{max}-Z)}{H_e}\right] \quad \text{(C17)}$$

where H is the scale height of the electron layer, one obtains

$$\frac{dn_e}{dZ} = \frac{n_e}{H_e} \quad \text{(C18)}$$

Incorporating equation (C18) into equations (C15) and (C16) allows them to be written

$$\frac{d\psi_d}{dZ} = \frac{\psi_d}{H_e} - \frac{\langle \sigma v \rangle n_e n_e(Z_{max}; t-t_d)}{v} \quad \text{(C19)}$$

$$\frac{d\psi_u}{dZ} = \frac{\psi_u}{H_e} - \frac{\langle \sigma v \rangle_{ne}}{v} n_e(Z_{min};\ t-t_u) \tag{C20}$$

Substituting equations (C12), (C19), and (C20) into equation (C14) allows the divergence term to be written,

$$-\nabla \cdot \varphi_n = \frac{n(Z,t)\langle \sigma v \rangle_{ne}}{(e^{-\psi_u} + e^{-\psi_d})} \left[\frac{v(e^{-\psi_u} - e^{-\psi_d})}{H_o \langle \sigma v \rangle_{ne}} + \frac{v(\psi_u e^{-\psi_u} - \psi_d e^{-\psi_d})}{H_e \langle \sigma v \rangle_{ne}} + e^{-\psi_u} n_e(Z_{min}; t-t_u) \right.$$

$$\left. + e^{-\psi_d} n_e(Z_{max}; t-t_d) \right] \tag{C21}$$

By hypothesis, the attenuation of the neutrals was very small for a traversal of the discharge, hence $\psi_u << 1$, $\psi_d << 1$. It will be shown later that for coherent oscillations to occur, one must have $H_e \approx H_o$ in the coherently oscillating region. Under these conditions, the first two terms within the brackets may be written

$$\frac{v(e^{-\psi_u} - e^{-\psi_d})}{H_o \langle \sigma v \rangle_{ne}} + \frac{v\left(\psi_u e^{-\psi_u} - \psi_o e^{-\psi_d}\right)}{H_e \langle \sigma v \rangle_{ne}} \approx \frac{v\left(\psi_d^2 - \psi_u^2\right)}{2H_o \langle \sigma v \rangle_{ne}} \tag{C22}$$

If n_e is an approximate spatial average of the electron number density, and T the transit time across the oscillating region, one can write $\psi_u \approx \psi_d \approx \hat{n}_e \langle \sigma v \rangle_{ne} T$, so that equation (C22) gives the approximate magnitude

$$\frac{v\left(\psi_d^2 - \psi_u^2\right)}{2H_o \langle \sigma v \rangle_{ne}} \approx \frac{n_e(Z_{max} - Z_{min})(\psi_d - \psi_u)}{2H_o} \tag{C23}$$

where one has made use of the relation

$$Z_{max} - Z_{min} = vT \tag{C24}$$

Equation (C23) implies that, so long as the thickness of the oscillating layer $Z_{max} - Z_{min}$ is not very much larger than the scale height H_o, the first two terms in the brackets of equation (C21) are smaller than the last two by a factor of magnitude $\psi_o - \psi_u$.

Since this term is much less than unity by hypothesis, the first two terms will therefore be dropped from subsequent developments.

Equation (C21) can then be written

$$-\nabla \cdot \varphi_n \approx n(Z, t)\langle \sigma v \rangle_{ne} \left[\frac{n_e(Z_{min}; t-t_u)}{1 + e^{-(\psi_d - \psi_u)}} + \frac{n_e(Z_{max}; t-t_d)}{1 + e^{-(\psi_u - \psi_d)}} \right] \tag{C25}$$

Since $\psi_u - \psi_d \ll 1$, one may expand the denominator to obtain

$$-\nabla \cdot \varphi_n \approx \frac{1}{2} n(Z, t)\langle \sigma v \rangle_{ne} \left[n_e(Z_{min}; t-t_u) + n_e(Z_{max}; t-t_d) \right] \tag{C26}$$

One can now invoke the argument used previously to replace the time-retarded electron number density with the time-averaged electron number density, since the velocity spread that is always present in actual cases will perform an averaging function. Experimental data relating to this assumption are presented in appendix E. Using a tilda to indicate a time average, we may write

$$n_e(Z_{min}; t-t_u) \rightarrow \tilde{n}_e(Z_{min}) \tag{C27}$$

$$n_e(Z_{max}; t-t_d) \rightarrow \tilde{n}_e(Z_{max}) \tag{C28}$$

Equation (C26) can therefore be written

$$-\nabla \cdot \varphi_n \approx \frac{1}{2} n(Z, t)\langle \sigma v \rangle_{ne} \left[\tilde{n}_e(Z_{min}) + \tilde{n}_e(Z_{max}) \right] \tag{C29}$$

If we define a time and space averaged electron number density

$$\hat{n}_e = \frac{1}{2} \left[\tilde{n}_e(Z_{min}) + \tilde{n}_e(Z_{max}) \right] \tag{C30}$$

equation (C29) can be written in terms of this average as

$$-\nabla \cdot \varphi_n = n(Z, t)\hat{n}_e\langle \sigma v \rangle_{ne} \tag{C31}$$

so that the neutral particle continuity equation may be written

$$\dot{n} = n(Z, t)\langle \sigma v \rangle_{ne} \left[\hat{n}_e - n_e(Z, t) \right] \tag{C32}$$

One can show by a physical argument virtually identical to that above that the electron continuity equation

$$\dot{n}_e = -\nabla \cdot \varphi_{ne} + n n_e \langle \sigma v \rangle_{ne} \tag{C33}$$

can be written in the symmetric form

$$\dot{n}_e = -n_e(Z, t)\langle \sigma v \rangle_{ne} \left[\hat{n} - n(Z, t) \right] \tag{C34}$$

where n is the time- and space-averaged neutral number density. This physical argument proceeds by replacing $n_e \rightarrow n$, and $n \rightarrow n_e$, and remembering that the signs of the arguments of the exponentials in equations (C4) and (C10) are positive, since the ionization process enhances the electron density in the oscillating region.

By following a derivation virtually identical to that in reference 11, one can show that when the peak-to-peak amplitude of $n_e(t)$ is small, the frequency of oscillation given by equations (C32) and (C34) is

$$\nu \approx \frac{\sqrt{\tilde{n}(Z)\tilde{n}_e(Z)}\ \langle \sigma v \rangle_{ne}}{2\pi} \tag{C35}$$

where $\tilde{n}(Z)$ is the time-averaged neutral number density at the position Z, and $\tilde{n}_e(Z)$ in the time-averaged electron number density at the same position. In order for the gas to oscillate coherently and with the same frequency, it is necessary that the product of densities be independent of position, that is,

$$\tilde{n}(Z)\tilde{n}_e(Z) \approx \text{constant} \tag{C36}$$

Since the neutral density of planetary and stellar atmospheres falls off exponentially with height above the surface, equation (C36) implies that the electron number density must increase exponentially with altitude, and with the same scale height, over a significantly thick layer of the planetary or stellar atmosphere. Small departures from a constant product of $\tilde{n}_e\tilde{n}$ may be allowable if $\langle \sigma v \rangle_{ne}$ varies with height in such a way that the frequency (equation (C35)) is maintained constant.

APPENDIX D

RELATION OF EXACT TO SMALL-AMPLITUDE SOLUTIONS

The exact solutions discussed above are in many ways not as satisfactory as the small-amplitude solutions presented in references 10, 11, and 13, since the latter gives the frequency $G(\eta)$ and the peak-to-peak amplitude as functions of η in closed form.

When n_{eo} is taken as the minimum value of $n_e(t)$, the parameter η used in the small amplitude solution is greater than unity, and the approximate solutions presented in reference 11 give a good qualitative account of the geometry and frequency of the waveform of $n_e(t)$. The peak-to-peak amplitude and $G(\eta)$ are given to within about 20 percent of the exact value by the small amplitude approximation.

The agreement between the small-amplitude approximation and the exact solutions is much less satisfactory for $\eta < 1.0$. If we denote the amplitude index used in the small-amplitude approximation by η_s, one can plot $G(\eta_s)$ and the peak-to-peak amplitude as a function of η_s for the relevant expressions in reference 11. This has been done in figure 8 for the parameter $G(\eta_s)$ and in figure 6 for the peak-to-peak amplitude. There is fair agreement of the exact with the small-amplitude solution between $0.80 \leq \eta_s \leq 1.0$, but the two diverge significantly below $\eta_s = 0.80$. This occurs because a mathematical artifact of the small-amplitude approximation restricts the small-amplitude solutions to the range $2/3 \leq \eta_s \leq 1.0$, while the exact solutions range over $0 \leq \eta_e \leq 1.0$.

The agreement of the exact with the small-amplitude solutions for $\eta < 1.0$ can be greatly improved by using the mapping between η_e and η_s given on figure 21. This mapping was obtained by requiring that the peak-to-peak amplitude of $y(t)$ for the value of η_e on the ordinate be equal to the peak-to-peak amplitude of $y(t)$ obtained from the small-amplitude approximation for the value of η_s given on the abscissa.

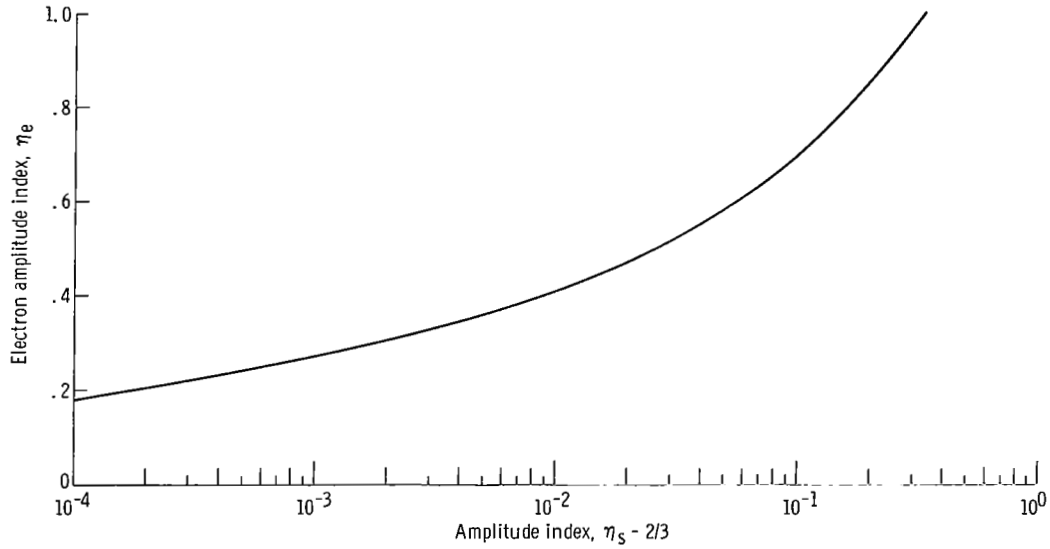

Figure 21. - Agreement between exact and small-amplitude solutions to equations (22) and (23) may be greatly improved by using heuristic transformation shown, which assumes that exact and small-amplitude solutions have same peak-peak amplitude. For a particular value of electron amplitude index used in exact solution one should use equivalent value of amplitude index used in small-amplitude approximation.

APPENDIX E

COHERENT OSCILLATION LIMITS AND NEUTRAL TRANSIT TIMES

In the derivation in appendixes B and C, it is shown that the transit time delays, which occur as a neutral particle moves with finite velocity across the discharge, play a fundamental role in the oscillation mechanism. These time lags appeared in equations (B18) and (C26) of these appendixes, in which the divergence term is written

$$-\nabla \cdot \varphi_n \approx n(t)\langle \sigma v \rangle_{ne} n_e(t-t_o) \tag{E1}$$

where t_o is the transit time delay associated with motion of a neutral particle of velocity $\bar{v}$ across a characteristic discharge dimension R. One may define a phase angle β by nondimensionalizing the time t with respect to the period of oscillation T,

$$n_e(t-t_o) \rightarrow n_e(\beta-\beta_o) \tag{E2}$$

where

$$\beta \equiv \frac{2\pi t}{T} = 2\pi\nu t \tag{E3}$$

and

$$\beta_o \equiv \frac{2\pi t_o}{T} = 2\pi\nu \frac{R}{\bar{v}} \tag{E4}$$

In appendixes B and C, it is argued that in actual applications, the velocity v is not a single value, but instead has a broad distribution of values. This in turn was used to justify replacing $n_e(t-t_o)$ by the time-averaged electron density, $\tilde{n}_e$. It is understandable that such an averaging would occur if $\beta_o \approx 2\pi$, since the transit time would then be comparable to the period of oscillation. One might also expect the discharge to no longer oscillate coherently and with the same phase if $\beta_o >> 2\pi$, since the neutrals would then, on the average, take many periods to move across the discharge. One might then expect a wave of ionization to propagate across the discharge, much like a moving striation. The oscillations might also be expected to disappear if $\beta_o << 2\pi$, since the maximum possible time delays would then not be sufficient to perform an averaging function, and a detailed balance would exist between the divergence and loss terms of the continuity equation.

It is therefore of interest to determine the range of β_o over which coherent, in-phase oscillations can be expected to occur. The data reported in reference 13 was accordingly reduced to determine the range of β_o for which coherent oscillations were observed in this experiment. The discharge radius was taken as R = 5.0 centimeters, and the average velocity v also appearing in equation (E4) was taken to be the most probable velocity of the molecules at a laboratory temperature of 283 K. The lowest and highest frequencies at which coherent in-phase oscillations were observed in deuterium, neon, and helium gas are listed in table III.

TABLE III. - OBSERVED RANGE OF TRANSIT-TIME PHASE ANGLE FOR EXPERIMENTAL DATA REPORTED IN REFERENCE 15

Species	Lowest observed frequency, Hz	Highest observed frequency, Hz	Neutral transit time, μsec	Lower limit of phase angle, β_{ol}		Upper limit of phase angle, β_{oh}, rad
				rad	deg	
D_2	340	50 500	37.7	0.0128	4.6	1.90
He	106	74 000	84.8	.0090	3.2	6.3
He	87	22 500	37.7	.0033	1.2	.85

Coherent oscillations may well have existed below the lowest frequencies shown, since these lower limits were determined by the disappearance of the light fluctuations into the background noise, and not by any loss of coherence. The upper limits were determined by the point above which propagating waves were observed in the discharge. The transit time of the neutrals across the discharge, in microseconds, is also given. The low and high values of $\beta_o/2\pi$ are also indicated.

It is, perhaps, surprising to find that the averaging process is effective when the phase angle β_{ol} is as small as 1.2^o. Evidently therefore, only very small time lags are necessary to destroy the detailed balance between production and loss processes, and thereby permit the oscillation to take place.

REFERENCES

1. Hewish, A ; Bell, S. J.; Pilkington, J. D. H.; Scott, P. F.; and Collins, R. A.: Observation of a Rapidly Pulsating Radio Source. Nature, vol. 217, no. 5130, Feb. 24, 1968, pp. 709-713.

2. Drake, F. D.; Gundermann, E. J.; Jauncey, D. L.; Comella, J. M.; Zeissig, G. A.; and Craft, J. D., Jr.: The Rapidly Pulsating Radio Source in Vulpecula. Science, vol. 160, no. 3827, May 3, 1968, pp. 503-507.

3. Lyne, A. G.; and Smith, F. G.: Linear Polarization in Pulsating Radio Sources. Nature, vol. 218, no. 5137, Apr. 13, 1968, pp. 124-126.

4. Duthie, J. G.; Sturch, C.; and Hafner, E. M.: Optical Pulse of a Periodic Radio Star. Science, vol. 160, no. 3826, Apr. 26, 1968, pp. 415-416.

5. Drake, F. D.; and Craft, H. D., Jr.: Pulse Structure of Four Pulsars. Science, vol. 160, no. 3829, May 17, 1968, pp. 758-760.

6. Lyne, A. G.; and Rickett, B. J.: Measurements of the Pulse Shape and Spectra of the Pulsating Radio Sources. Nature, vol. 218, no. 5139, Apr. 27, 1968, pp. 326-330.

7. Craft, H. D., Jr.; Comella, J. M.; and Drake, F. D.: Submillisecond Radio Intensity Variations in Pulsars. Nature, vol. 218, no. 5147, June 22, 1968, pp. 1122-1124.

8. Drake, F. D.: Pulse Structure of the Pulsating Radio Source in Vulpecula. Science, vol. 160, no. 3826, Apr. 26, 1968, pp. 416-419.

9. Gold, T.: Rotating Neutron Stars as the Origin of the Pulsating Radio Sources. Nature, vol. 218, no. 5143, May 25, 1968, pp. 731-732.

10. Roth, J. Reece: Periodic, Small-Amplitude Solutions to the Spatially Uniform Plasma Continuity Equations. NASA TN D-4472, 1968.

11. Roth, J. Reece: A New Mechanism for Low-Frequency Oscillations in Partially Ionized Gases. Phys. Fluids, vol. 10, no. 12, Dec. 1967, pp. 2712-2714.

12. Roth, J. Reece: Experimental Observation of Nonlinear Oscillations Governed by the Plasma Continuity Equations. Am. Phys. Soc. Bull., vol. 13, no. 2, Feb. 1968, p. 282.

13. Roth, J. Reece: Experimental Observation of Oscillations Described by the Continuity Equations of Slightly Ionized Denterium, Neon, and Helium Gas. NASA TN D-4950, 1968.

14. Lotz, Wolfgang: Electron-Impact Ionization Cross-Sections and Ionization Rate Coefficients for Atoms and Ions. Astrophys. J. Suppl. Ser., vol. 14, no. 128, May 1967, pp. 207-238.

15. Lotz, Wolfgang: Electron Impact Ionization Cross-Sections and Ionization Rate Coefficients for Atoms and Ions from Hydrogen to Calcium. Rep. IPP-1/62, Institut fur Plasmaphysik G. M. b. H., May 1967.

16. Lotka, Alfred J.: Undamped Oscillations Derived from the Law of Mass Action. J. Am. Chem. Soc., vol. 42, no. 8, Aug. 1920, pp. 1595-1599.

17. Volterra, V.: Variations and Fluctuations of the Number of Individuals in Animal Species Living Together. International Council for the Exploration of the Sea. Journal du Conseil, vol. 3, 1928, pp. 1-51.

18. Davis, Harold T.: Introduction to Nonlinear Differential and Integral Equations. Dover Publications, Inc., 1962, p. 95.

19. Roth, J. Reece; Freeman, Donald C., Jr.; and Haid, David A: Superconducting Magnet Facility for Plasma Physics Research. Rev. Sci. Instr., vol. 36, no. 10, Oct. 1965, pp. 1481-1485.

20. Roth, J. Reece: Modification of Penning Discharge Useful in Plasma Physics Experiments. Rev. Sci. Instr., vol. 37, no. 8, Aug. 1966, pp. 1100-1101.

21. Roth, J. Reece: Steady-State, Hot-Ion Particle-Injection Scheme for Mirror Machines. Am. Phys. Soc. Bull., vol. 11, no. 4, June 1966, p. 465.

22. Roth, J. Reece; and Clark, Marion: Analysis of Integrated Charged Particle Energy Spectra from Gridded Electrostatic Analyzers. NASA TN D-4718, 1968.

23. Allen, Clabon W.: Astrophysical Quantities. Second ed., Oxford Univ. Press, 1963.

24. Morrison, Philip: Extra-Solar X-Ray Sources. Annual Review of Astronomy and Astrophysics. Vol. 5. L. Goldberg, ed., Annual Reviews, Inc., 1967, pp. 325-350.

25. LeLevier, R. E.; and Libby, L. Marshall: Galactic X-Rays: Variable Sources in Hydromagnetic Waves. Science, vol. 160, no. 3835, June 28, 1968, pp. 1447-1449.

26. Troitskaya, V. A.; and Gul'elmi, A. V.: Geomagnetic Micropulsations and Diagnostics of the Magnetosphere. Space Sci. Rev., vol. 7, no. 5/6, 1967, pp. 689-768.

27. Campbell, W. H.: Studies of Magnetic Field Micropulsations with Periods of 5 to 30 Seconds. J. Geophysic. Res., vol. 64, no. 11, Nov. 1959, pp. 1819-1826.

28. Annexstad, John O.; and Wilson, Charles R.: Characteristics of Pg Micropulsations at Conjugate Points. J. Geophysic. Res., vol. 73, no. 5, Mar. 1, 1968, pp. 1805-1818.

29. Johnson, Francis S.: Planetary Atmospheres 1958-1964. NASA SP-98, 1966, p. 25.

NASA-Langley, 1969 —— 25 E-4603